



# CHORUS

This is the accepted manuscript made available via CHORUS. The article has been published as:

## Domain structure and magnetic pinning in ferromagnetic/superconducting hybrids

V. Vlasko-Vlasov, A. Buzdin, A. Melnikov, U. Welp, D. Rosenmann, L. Uspenskaya, V. Fratello, and W. Kwok

Phys. Rev. B **85**, 064505 — Published 7 February 2012

DOI: [10.1103/PhysRevB.85.064505](https://doi.org/10.1103/PhysRevB.85.064505)

## Domain structure and magnetic pinning in ferromagnetic/superconducting hybrids

V. Vlasko-Vlasov<sup>1</sup>, A. Buzdin<sup>2</sup>, A. Melnikov<sup>3</sup>, U. Welp<sup>1</sup>, D. Rosenmann<sup>1</sup>, L. Uspenskaya<sup>4</sup>,  
V. Fratello<sup>5</sup>, W. Kwok<sup>1</sup>

<sup>1</sup>Argonne National Laboratory, Argonne, IL 60439, USA

<sup>2</sup>CPMOH, Institut Universitaire de France and Université Bordeaux I, UMR 5798 CNRS, F-33405 Talence, France

<sup>3</sup>Institute of Physics of Microstructures RAS, GSP-105, 603950 Nizhny Novgorod, Russia

<sup>4</sup>Institute of Solid State Physics RAS, 142432 Chernogolovka, Russia

<sup>5</sup>Integrated Photonics, Inc., Hillsborough, NJ 08844, USA

### Abstract

Magnetic patterns in three iron-garnet films with different magnetic properties covered with 100 nm superconducting Nb film are studied using magneto-optical imaging technique. In all samples the strong coupling between ferromagnetic domains and vortices noticeably modifies the magnetization process. However, depending on the type and width of the magnetic domains we observe different flux dynamics in the Nb film. Wide domains give rise to a combined domain structure and type-I like superconducting response resulting in enhanced attenuation of the flux motion due to cooperative pinning of vortices and magnetic domain walls. These combined domains strongly shrink in the ac fields due to a dynamic instability triggered by oscillating domain walls. Combined domains formed on narrow magnetic domains do not shrink but they guide the motion of vortices and in turn align in the vortex motion direction. This introduces superconducting current anisotropy due to strong pinning on the magnetic domain walls. Irregular magnetic domain structures with immobilized domain walls stochastically modify the vortex entry patterns. The presence of magnetic domains essentially arrests thermo-magnetic avalanches in the superconducting layer. The studied magnetic pinning has a good potential for slowing down vortices in high- $T_c$  superconductors.

### Introduction

Coupling of mutually exclusive order parameters, such as superconductivity (SC) and ferromagnetism (FM), offers a whole set of fascinating effects and novel phenomena. They include the appearance of triplet superconductivity [1], variations of the SC transition temperature ( $T_c$ ) [2-4], fine scale order parameter modulations [5-6], cryptomagnetic structures [7],  $\pi$  and random angle junctions [8], long-range proximity [9-11], tunable reentrant superconductivity [12], and magnetic pinning [13-14]. A comprehensive discussion of mentioned effects can be found in recent reviews [15-20]. Among those phenomena the magnetic pinning is probably the less studied effect in spite of its key practical potential for power and other SC applications requiring high critical currents such as superconducting cables, magnets, electric machines, energy storage devices and so on. In fact, theoretical estimates show that the SC critical currents based on the magnetic pinning can reach the depairing current value and the introduction of the magnetic pinning in high-temperature superconductors is the only way to arrest vortex dynamics at high temperatures [13].

Vortex dynamics is the general feature of type-II SCs controlling their transport and magnetic response. Independent of the nature of pairing, composition of the materials, and

peculiarities of their H-T phase diagram, it is the emergence of the vortex motion, which limits the current carrying ability of SC components. Therefore, the major effort in SC science and technology is devoted to the understanding of the vortex matter and finding effective ways of its immobilization. The usual approach is to generate point-like (inclusions, vacancies, precipitates), linear (columnar defects, second phase nanorods), or planar (grain boundaries, stacking faults) poorly superconducting defects [21-23]. Vortices residing on the defects gain the condensation energy  $H_c^2/8\pi$  ( $H_c$  is the thermodynamic critical field) in the volume  $v_d$  of the vortex core/defect intersection, which defines the core pinning potential  $U_c$ . The critical field is  $H_c = \Phi_0/2\sqrt{2} \pi \xi \lambda$ , where the flux quantum  $\Phi_0$  is a constant, while the coherence length  $\xi$  and the penetration depth  $\lambda$  strongly diverge with temperature ( $\xi \sim \lambda \sim (T_c - T)^{-1/2}$ ) [21]). Thus for defects of reasonably small sizes  $U_c$  becomes inefficient at higher temperatures causing a dramatic drop of the critical currents. These effects are particularly harmful in the case of high- $T_c$  superconductors, where catastrophic creep of vortices at  $T \sim U_c$  wipes out all the advantages of the high transition temperature.

Magnetic pinning was proposed as an alternative to the core pinning [13]. To realize the magnetic pinning one has to create strong magnetic gradients, for example by using artificial arrays of magnetic particles (“magnetic dots” [19-20] or rods [24-25]) or by manufacturing the SC layer on a FM substrate with natural magnetic inhomogeneities due to domains [13, 26-33]. The scale of the magnetic pinning potential  $U_m$  will be defined by the Zeeman coupling of the vortex flux and magnetization  $-\mathbf{M}\Phi_0$  [17], which is minimum at the mutual alignment of  $\mathbf{M}$  and  $\Phi_0$ . Accounting that the ferromagnetic Curie temperature is usually much larger than  $T_c$ ,  $M$  and thus  $U_m$  may be considered as  $T$  independent and should be much higher than  $U_c$  at  $T \sim T_c$ .

In the present work we study remagnetization processes in a SC film sputtered simultaneously on three FM substrates with different magnetic anisotropy, magnetization, and domain structure (DS). They all show strong interactions between vortices and magnetic domains but reveal different effects of the magnetic pinning depending on the type of the DS in the FM substrate. When domains in the FM film with perpendicular anisotropy are wider than the FM film thickness, the combined structure of vortices coupled to the FM domains forms. It modifies the magnetic response of the hybrid and essentially attenuates the flux mobility. In bilayers with wide domains the combined structure is strongly refined in the AC field due to a novel dynamic instability in the system. The synergetic action of the pinning of vortices in the SC layer, pinning of domain walls in the FM layer, and domain wall/vortex coupling in the combined structure strongly impedes the magnetic flux dynamics and arrests thermo-magnetic instabilities in the hybrid. In the case of narrow FM domains, the flux dynamics is also retarded by domain walls, which direct the vortex motion along them and impede the vortex motion across the walls. In turn, moving SC vortices align the FM domains. The width of the narrow domains practically does not change in the AC fields. In hybrids with irregular domain structures the magnetic pinning is weaker, but it still defines the shape of the flux penetration front. We propose a theoretical model, which describes observed peculiarities in the magnetic behavior of the SC/FM bilayers and explains the dynamic instability of the combined DS in the AC field initiated by vortex/antivortex collapse around oscillating domain walls. This paper is an extension of our previous work published in [32].

## Experiment

Three single-crystal rare-earth iron garnet films of the composition  $RE_3(Fe, Ga)_5O_{12}$  with

different magnetization, anisotropy, thickness, and domain structure, grown on GdGa garnet (GGG) wafers, were used as magnetic substrates. RE is a combination of several rare-earth ions forming the anisotropy and together with Ga substitution, defining the total magnetic moment of the ferrimagnetic garnets [34]. These materials are robust dielectrics with a wide energy gap, which allows us to avoid proximity effects and directly study peculiarities of the magnetic pinning in our samples. Our garnet films had  $\sim 5 \times 5 \text{ mm}^2$  surface area. Their magnetic parameters were extracted from magnetization curves measured using SQUID in fields perpendicular and parallel to the film and from the width of stripe domains as discussed below. Then a 100 nm Nb layer was sputter-deposited on a half of each garnet film through a stencil mask at  $6.5 \times 10^{-10}$  Torr base pressure in 4 mTorr Ar atmosphere. In the same sputtering run the same Nb film was deposited on a glass slide as a reference sample. The diamagnetic response of the Nb film measured by SQUID showed the sharp SC onset temperature  $T_c = 8.5 \text{ K}$  and  $\sim 0.2 \text{ K}$  transition width defined at 95% of the maximum negative signal. Placing the edge of the SC film in the center of the samples allowed us simultaneously to image the domain structure in bare and Nb covered parts of the sample and clearly distinguish the magnetization process in the hybrid from that in the garnet. Imaging was performed by the magneto-optical indicator technique [35] using garnet films with in-plane anisotropy, large Faraday rotations and high response to perpendicular magnetic fields. The indicator film is placed on the sample and visualizes the normal component of magnetic fields ( $B_z$ ) on the sample surface. It yields  $B_z$  maps above domains in the FM and SC/FM areas and reveals the vortex distribution in the Nb film during remagnetization. In the images below the intensity of the contrast increases with increasing  $+B_z$  (bright contrast reveals positive vortex density) and decreases with increasing  $-B_z$  (dark contrast reveals negative vortex polarity).

## Results and discussion.

Experimental observations of flux patterns in the Nb layer on different garnet films.

### 1. Garnet film with wide domains.

Below we consider domains as *wide* if their width to film thickness ratio  $D/d_F$  is noticeably larger than 1 and *narrow* if  $D/d_F < 1$ . The first garnet film with perpendicular magnetic anisotropy was  $3.9 \text{ }\mu\text{m}$  thick and at room temperature had  $6.6 \text{ }\mu\text{m}$  wide labyrinth domains. Magnetization loops for this film acquired at different  $T$  in fields perpendicular to the film plane are presented in Fig.1a. The magnetic moment and coercivity of the film increase upon cooling resulting in rectangular  $M(H)$  loops already at  $250 \text{ K}$ . Measurements of the in-plane magnetization perpendicular to the film easy axis required magnetic fields up to  $\sim 10^4 \text{ Oe}$ , which yielded a large signal from the GGG substrate allowing estimates of the saturation field but compromising the accurate value of the film contribution to the total magnetic moment below  $250 \text{ K}$ . At larger  $T$  the in-plane magnetization curves provided correct values of  $M$  (see Fig.1b). We used the perpendicular field data to build the  $T$  dependence of the saturation magnetization ( $M_s$ ) presented in Fig.2. It shows that  $M_s$  goes through a maximum at  $\sim 160 \text{ K}$ , drops to a minimum at  $\sim 40 \text{ K}$ , and then sharply increases below  $30 \text{ K}$ . This is a typical behavior observed in garnets with two unequal and oppositely magnetized iron sublattices (Fe ions in octahedral and tetrahedral oxygen environment) and RE spins in the dodecahedral sublattice [34]. The reduction of  $M_s$  towards  $40 \text{ K}$  signifies a partial compensation of the sublattice contributions, while the low- $T$  increase of magnetization is due to the strong paramagnetism of the rare earth. Note, that even at low  $T$  the

maximum increase of  $M_s$  is only  $\sim 30\%$  and we can consider  $M_s$  constant below the critical temperature of Nb (8.5K).

With decreasing  $T$  the domains in the garnet film gradually expand. To obtain the equilibrium domain structure (DS) hindered by the increasing pinning of domain walls (DW), it is necessary to apply and slowly reduce an AC magnetic field. In this traditional procedure the amplitude  $h$  and frequency  $f$  of the required AC field depend on temperature. A similar “shaking” procedure equilibrates vortices at  $T < T_c$  (e.g.[34]). By directly observing the DW oscillations we determined appropriate  $h$  and  $f$  at 4.2K and used these values at all  $T$ . Fig.3 shows the temperature variations of the equilibrated domain width  $D(T)$  after application and reduction of  $h=50$  Oe at  $f=17$  Hz. The domain width in the bare garnet film increases nearly 4 times down to 40 K and then saturates around  $\sim 27$   $\mu\text{m}$ .

The equilibrium domain width in magnetic films with perpendicular anisotropy and large quality factors  $Q = K/2\pi M_s^2$  ( $K$  is the uniaxial anisotropy constant) is well described by experimentally proven formulas [37-39] allowing the extraction of the important magnetic parameters, such as  $M_s$  and the dipolar length  $l_c = \frac{\sqrt{AK}}{\pi M^2}$  (here  $A$  is the exchange constant) using the value of  $D$  and the domain collapse field  $H_{col}$ . At  $Q \gg 1$   $D$  is defined by an implicit formula [37-38]:

$$\frac{l_c}{d_F} = \frac{4}{\pi^3} p^2 F(p) \quad (1)$$

with

$$F(p) = \sum_{k=1}^{\infty} \frac{1}{k^3} [1 - (1 + \pi k p) e^{-\pi k p}], \quad p = D/d_F, \quad k = 2n+1, \quad \text{and } n=0,1,2,\dots$$

The collapse field to a good accuracy is presented by the Thiele function [39]:

$$H_{col} = 4\pi M_s [1.0016 - 1.63 \sqrt{\frac{l_c}{d_F}} + 0.535 \frac{l_c}{d_F} + 0.152 \left(\frac{l_c}{d_F}\right)^2] \quad (2)$$

Taking the room temperature domain width  $D=6.6$   $\mu\text{m}$  and  $d_F=3.9$   $\mu\text{m}$  we obtain  $l_c=0.87$   $\mu\text{m}$  from (1) and find  $M_s=11.8$  G from (2) using the experimental value of  $H_{col}=53$  Oe. Then from the measured in-plane saturation field  $H_s=2K/M_s=3200$  Oe we get the anisotropy constant  $K=1.9 \cdot 10^4$  erg/cm<sup>3</sup> and the quality factor  $Q=21.36$ . Finally, from  $l_c$  we obtain  $A=0.8 \cdot 10^{-7}$  erg/cm and the domain wall energy  $\sigma_{DW} = 4\sqrt{AK} = 0.156$  erg/cm<sup>2</sup>. An account of the finite  $Q$  using exact formulas of [38] practically does not change the value of  $l_c$  and other parameters.

At 8K we determine  $M_s=15.9$  G and  $K=6 \cdot 10^4$  erg/cm<sup>3</sup> from magnetic measurements and using the average domain width  $D=26.9$   $\mu\text{m}$  calculate  $l_c=2.49$   $\mu\text{m}$  which yields the exchange constant  $A=2.1 \cdot 10^{-6}$  erg/cm. The increase of the domain wall energy  $\sigma_{DW}(8K)/\sigma_{DW}(300K)=5$  is larger than the increase of the magnetostatic energy  $M_s^2(8K)/M_s^2(300K)=1.8$  which explains the observed expansion of domains.

Imaging  $B_z$  distributions near the boundary of the Nb film allowed us to compare directly the behavior of the DS in the bare garnet and in the SC/FM bilayer. At  $T$  slightly below  $T_c \sim 8.5$ K the DS was the same on both sides of the SC edge even after application of the AC field. Such a behavior can be referred to the suppression of the SC order by the stray fields of domains. We did not observe any difference in the magnetic contrast above the domains (i.e. the stray fields are the

same) in the bare garnet and in the Nb covered areas, which supports this explanation. It shows that close to the superconducting transition the stray fields are not screened by the Nb film but are maintained through the nucleation of appropriate densities of vortices and antivortices in neighboring domains. At  $\sim 2\text{K}$  below  $T_c$  however, the equilibrated domains under the Nb layer start narrowing compared to the bare garnet film as shown in Fig.4. The edge of the Nb film in Fig.4 is marked by the broken line behind which there is a transition band in the SC area where domains change their width from that of the bare FM film ( $D_M$ ) to a smaller value in the FM/SC area ( $D_S$ ). The transition band shrinks at lower T. Deeper in the SC region, where the AC field is screened by Nb, wider domains may remain frozen from larger temperatures. The AC field amplitude required for shaking domains in the SC region at lower T is larger than that for the bare garnet film even though there is a strong concentration of the field near the SC film edge. In this case the vortex pinning effectively increases the coercivity of domain walls in the SC area. The maximum shrinkage of the domains in the Nb area is  $D_M/D_S \sim 3$  and the average ratio below 6K is  $\sim 1.9$ . The latter is close to the domain shrinkage of 2.1 reported for a magnetic garnet film covered with a 300 nm Pb layer [40-41]. Such a value is well above 1.2, the maximum ratio achievable at the total Meissner screening of the stray fields of narrow ( $D < d_F$ ) FM domains [42-46] and it is in contrast to the expected expansion of wide domains ( $D > d_F$ ) [43] as is discussed below. This indicates that the screening effects are negligible, in accordance with our observations of  $B_z$  below  $T_c$  in domains over the Nb area where it is supported by vortices, and other mechanisms control the domain behavior.

At temperatures around  $\sim 7 - 6\text{ K}$ , when the vortex pinning is relatively weak, we observe a partial alignment of the AC equilibrated domains perpendicular to the SC edge (Fig.5a). This orientation coincides with the direction of the vortex entry from the Nb edge and the effect can be treated as the alignment of the magnetic domain walls by moving vortices. Earlier, we found the directional penetration of vortices in a SC NbSe<sub>2</sub> crystal and thick Pb film along parallel stripe domains in a FM permalloy capping layer [30-31]. Our new observation shows that not only vortices can move preferentially along the domains guided by the strong DW pinning potential but also the vortex motion can align the domain walls. Below we show that this effect is more pronounced in hybrids with narrow domains. Actually, the situation is more complicated. In the case of a strong coupling between the FM domains and SC vortices these two subsystems should not be considered as individual but rather as a unity forming new *combined domain structure* [17]. The strong coupling appears when magnetization in domains is perpendicular to the film surface so that FM domains and vortices polarized along the magnetic moments in domains form a new merged entity with new characteristic dimensions and properties. This situation is different from the pinning by magnetic nanoparticles in SC films, when the main coupling energy due to the stray fields,  $H_s$ , is  $U_{MS} = -\Phi_0 H_s d_s / 4\pi$ , where  $d_s$  is the thickness of the SC layer. When vortices are coupled directly to the magnetization of domains in a FM film of thickness  $d_F$ ,  $U_M = -\Phi_0 M d_F$ , which can have much larger value than  $U_{MS}$ . Counter-intuitively, this coupling occurs even in the absence of the stray fields.

The appearance of the combined structure results in a stronger attenuation of the magnetic flux dynamics due to the synchronization of the vortex pinning in the SC layer, pinning of the domain walls in the FM film, and mutual vortex/domain wall pinning [32]. Also it modifies the electromagnetic response of the hybrid making it similar to that in a type-I superconductor, where magnetization occurs through the nucleation and expansion of the normal domains at the expense of shrinking SC domains. In our samples the remagnetization process also advances through the

growth of combined domains polarized along the external field and contraction of oppositely polarized neighboring domains.

Fig.5 illustrates the DC remagnetization of the sample after the AC equilibration at 6.2K. In Fig.5b-e domains polarized along the field (bright) in both bare garnet (left) and garnet/Nb regions (right) expand at the expense of oppositely magnetized domains (dark) at increasing field. However, in the bare garnet this process goes faster (Fig.5c-e). To some extent, this is due to the partial screening of the field by the SC layer. However, the main reason of the stronger magnetization delay in the Nb area is the enhanced pinning of the combined domain walls. If the maximum applied field leaves narrow domains of the opposite polarity (as in Fig.5e) they grow back at decreasing field. Fig.5f shows that under the superconductor combined domains grow faster and are wider than in the bare garnet film. On one hand, this expansion of combined domains is due to the fast decay and inversion of the magnetic induction near the edge of the SC film in the decreasing external field [47, 48]. On the other hand, the oppositely polarized domains efficiently reduce their energy (by  $U_M$ ) when filled with vortices of the same polarity and act as generators of “negative” vortices. They are wider near the edge of the Nb film and acquire a branching structure (Fig.5g-h), which creates the increasing negative gradient of an average  $B_z$  towards the edge. The situation is similar to a single SC film where such a gradient is produced upon ramping down the field by the decreasing and inverting vortex density at the edge. So, the motion of the combined domains not only implements the remagnetization of the hybrid but also forms proper average flux gradients. In this case local currents in the SC layer flow in an intricate pattern of wiggling lines bent at the domain walls and carrying the maximum current density along them. However, the average current is directed along the Nb edge as in a usual SC critical state.

A different scenario occurs after the garnet film is saturated in a large magnetic field. The perpendicularly magnetized FM layer does not produce any stray fields (except at the edge) and thus a picture similar to that of a bare SC film in a homogeneous normal field should be observed. Although, even in the absence of stray fields normally magnetized substrate may attract similarly polarized vortices ( $U_M < 0$ ). Fig.6 illustrates such a process at 6.2K. We start with an initial state with combined domains obtained after application and slow decrease of a DC field  $H = -70$  Oe (compare Fig.6a with Fig.5h obtained after decreasing field from  $H = +89$  Oe). At increasing positive field (Fig.6a-d) the magnetization goes through the extension of domains polarized along  $\mathbf{H}$  and shrinkage of oppositely polarized domains as in Fig.5a-e. A new feature is the formation of circular spots at the ends of branched domains (Fig.6b-c). They are not observed in the bare garnet film and appear due to the interplay between the local magnetostatic energy of the combined domains containing vortices and increased effective energy of their domain walls carrying enhanced screening currents in the SC layer. At decreasing field after the sample is saturated by  $H = +800$  Oe the sample shows an inhomogeneous exit of vortices near the edge of the Nb film (Fig.6e-f). This picture is typical for a single SC layer with defects [49]. The average induction decreases and changes sign near the edge due to inverted screening currents supporting the trapped vortices in the SC film [47-48]. The garnet layer remains saturated at  $H = 0$  and no domains form in the Nb area. The garnet is magnetized in the positive  $H$  direction and supports the positive trapped flux in the Nb film but hinders the entry of negative vortices at the SC edge, which would occur at switching off the field in a bare SC layer. Such a suppression of negative vortices is due to their energy exceeding that of positive vortices by  $2\Phi_0 M$ .

At following application of the negative field we first observe the increase of the negative vortex density in the Nb area (contrast decreases in Fig.6g) and then, at  $H \sim -50$  Oe, an abrupt appearance of narrow bright lines (positive domains) as shown in Fig.6h. Further increase of the

negative H results in their collapse at  $H \sim -120$  Oe and saturation of the garnet in the negative field direction. Reduction of the negative field to zero (Fig.6i) yields the very same pattern (but of inverted polarity) as after application of the saturating positive field (Fig.6f) confirming that the flux inhomogeneity is defined by structural imperfections in the Nb film. The following ramping of the positive field results in a jumpwise emergence of narrow negative domains (dark lines in Fig.6j). Such a sudden arrival of narrow negative domains in the positive field and narrow positive domains in the negative field is a result of the nucleation and fast expansion of domains polarized along H in the garnet film saturated against the field direction. As a result, only narrow domains polarized against H are left. This corresponds to the rectangular magnetization curves of the garnet at low temperatures. However, these domains have different shape in the bare garnet and in the Nb covered area where they carry vortices modifying their dynamics. Within the field range where narrow domains do not collapse the remagnetization of the hybrid always occurs through the expansion/contraction of the combined domains (Fig.6k-l).

Qualitatively similar remagnetization process is observed at lower temperatures (Fig.7). However, in this case the vortex pinning is strongly increased causing the appearance of thermomagnetic avalanches (TMA) [50-53] in addition to the combined domain motion. They bring jump-wise branching discharge of antivortices into vortex filled areas forming macroscopic irregular branching patterns of bright -vortex and dark -antivortex stripes as shown on the right in Figs.7e-h.

We found that the presence of combined domains is significantly suppressing the appearance of TMA compared to the bare SC film. Simultaneous imaging of remagnetization patterns in the Nb/garnet sample and the same Nb film on glass showed that under the action of AC fields TMA occur in the bare Nb film at noticeably larger temperatures than in the hybrid sample (Fig.8a,c). In fact, TMA appear in the bare Nb film at  $\sim 6$ K, while in the hybrid with domains they were not observed down to  $\sim 4.7$ K. Thus, in spite of a stronger pinning in hybrids the boundaries of combined domains efficiently arrest the jumps of magnetic flux.

## 2. Garnet film with narrow domains.

The second garnet film with perpendicular anisotropy was  $1.6 \mu\text{m}$  thick and at room temperature had an average width of labyrinth domains  $D=1.15 \mu\text{m}$ . A few magnetization loops of this film in the perpendicular field are presented in Fig.9a and the appropriate  $M(T)$  dependence is shown in Fig.9b. Remarkably, in a wide range of temperatures the ascending branches (Up arrow) of the  $M(H)$  loops at different temperatures practically coincide, except that the saturation level ( $M_s$ ) increases with decreasing T. This shows that the coercivity for the domain wall motion is small. Moreover, at higher T ascending and descending branches (Up and Down arrows) also coincide. Only at  $T < \sim 100$ K the field of departure from the saturation ( $M=M_s$ ) on the descending branch, corresponding to the nucleation of inverse domains at decreasing H, shifts to smaller values compared to the domain collapse field on the ascending branch. Such a behavior indicates that the domain nucleation barrier is small in a wide temperature range, but it increases at cooling the sample and results in a hysteretic opening of the loops. After the domains are nucleated they spread over the sample without retardation. In-plane magnetization curves (Fig.9c) saturate at progressively increasing fields at decreasing T, reflecting the increase of the magnetic anisotropy. Estimates of the magnetic constants obtained as described in the previous paragraph using the domain width D, collapse field  $H_{\text{col}}=300$  Oe, and in-plane saturation field  $H_s=1655$  Oe at  $T_{\text{room}}$  yield  $l_c=0.072 \mu\text{m}$ ,  $M_s=35.1$  G,  $K=2.9 \cdot 10^4 \text{erg/cm}^3$ ,  $Q=3.75$ ,  $A=0.27 \cdot 10^{-7}$

erg/cm and the domain wall energy  $\sigma_{DW} = 4\sqrt{AK} = 0.11 \text{ erg/cm}^2$ . At low temperatures domains expand and at 6K after the AC equilibration have the average width  $D=2.88 \text{ }\mu\text{m}$ . From magnetic measurements we find  $M_s=63 \text{ G}$  and  $K=2.68 \times 10^5 \text{ erg/cm}^3$ , which yields  $l_c=0.69 \text{ }\mu\text{m}$  and  $\sigma_{DW}=3.4 \text{ erg/cm}^2$ . As in the previous case, the stronger increase of the domain wall energy compared to the magnetostatic energy defines the low temperature expansion of domains.

Although the  $D/d_F$  ratio is slightly larger than 1 at low T, is still small compared to that for the wide domains discussed in the previous paragraph, which causes new peculiarities of the flux dynamics in the sample. First, the equilibration of domains requires larger AC fields. For  $H_{AC} < \sim 200 \text{ Oe}$  (17 Hz) DWs are totally immobilized at  $T < 8\text{K}$ . This can be explained by the increased collective pinning of FM DWs strongly coupled through the magnetostatics of narrow domains. Second, we do not observe any difference in the equilibrated domain width in the bare garnet and over the Nb film down to lowest T of 4.3K. This is in accordance with small changes of DS predicted for hybrids with narrow domains as discussed below. At the same time, after application of the AC field domains become clearly aligned perpendicular to the Nb edge in the SC area, while the labyrinth DS forms in the bare garnet film (Fig.10 a). Such a behavior reveals the effect of moving vortices on the orientation of domains walls. It becomes more pronounced in the case of narrow domains due to their cooperative motion induced by stronger magnetostatic coupling between domain walls and their higher density. Accounting for the fact that the main impact on the DWs is produced by vortices moving near them, the ramification of domains should result in a larger total DW/vortex interaction area, which assists “combing” of DWs by vortices entering and exiting across the SC edge in the AC field. Note, that labyrinth domains are a preferred DS in FM films with the perpendicular anisotropy because of their smaller magnetostatic energy compared to parallel stripes. So, the alignment of DWs is obviously associated with the impact of vortices.

After application of a larger AC field, domains in the SC area lose their regularity but on the average still align perpendicular to the Nb edge (Fig.10b). In the DC field this domain structure starts changing only in fields  $>200 \text{ Oe}$  showing local expansion of domains at  $H > 250 \text{ Oe}$  (bright spots in Fig.10c-d). They gradually grow leaving narrow domains (dark) polarized against the field, which are more irregular in the bare garnet area (Fig.10e-f). After saturation at  $\sim 600 \text{ Oe}$ , further reduction of H results in the nucleation of inverse domains already in a relatively large positive field. These domains nucleate and grow preferentially in the SC area upon decreasing and changing the polarity of H (dark lines in Fig.11a-c). Only in a negative field  $H \sim -80 \text{ Oe}$  do the density of domains and the width of positive and negative domains in the bare garnet and Nb covered areas become comparable (Fig.11d-e). Fig.11b, taken after reduction of H to zero, illustrates a peculiar effect of reverse domains on the structure of the trapped flux in the hybrid. Here ridges of the enhanced vortex density are observed along the center lines of wide trapped flux domains (positive). Their images are brighter in the middle and lose the intensity towards narrow dark lines of negative domains. Similar “roof” patterns of the trapped flux with the vortex density dropping and changing sign near the edge are usually observed in the SC strips. However, in our sample the trapped flux in bright domains exits upon the reduction of H not just to the edge of the SC film but to the nearest negative (dark) domains, which serve as a vortex drain network. These domains generate antivortices partially annihilating the trapped flux vortices and expand upon filling with negative flux. Under the superconductor the negative domains are slightly wider than in the bare garnet due to the larger demagnetizing fields induced by trapped positive vortices. Here SC currents in the Nb film flowing along the boundaries of combined domains form loops supporting the trapped flux in the positive domains. In some

regions near the SC edge and far from the reverse domains vortices exit (negative vortices enter) through the edge as usual (Figs.11b-c), resulting in a traditional balloon like pattern due to defects [35, 49, 54].

Upon ramping up of a negative field the negative combined domains multiply and their width slightly reduces. However, in contrast to the initial advanced nucleation of domains, in the SC area this process goes slower than in the bare garnet film when the domains are refined (Fig.11d). This can be referred to the enhanced cooperative pinning in the coupled domain/vortex system as discussed earlier. At further increasing negative field, negative and positive domains acquire the same width and form the labyrinth pattern (Fig.11e). Finally, domains polarized against the field shrink and collapse (Fig.11f) as described above.

The tendency towards the preferred nucleation of the inverse domains in the SC area shows itself also during the increase of the AC field applied to the magnetized sample. Increasing  $H_{AC}$  in the absence of the DC field should facilitate the return to the demagnetized equilibrium state. This process requires the nucleation and motion of the inverse domains in the ferromagnet and in the SC region it involves also the depinning of vortices. So one could expect that under the Nb film the process should be delayed. In contrast, at small negative DC fields we observe the reversal process going faster in the SC area. This can be explained accounting that trapped vortices produce stray fields enhancing the magnetostatic energy and promoting the formation of inverse domains while the magnetic coupling  $U_M$  reduces the energy of the emerging combined negative domains. At the same time, the energy required for generation of antivortices in the reverse domains is compensated by the annihilation of trapped vortices. Altogether, these factors induce a preferential nucleation of domains in the SC area.

Fig. 12 illustrates the development of multiple domains in the increasing AC field after the sample was partially saturated by application and switching off  $H_{DC}=500$  Oe at 4.5K. An amplitude of  $H_{AC}$  (17 Hz) is continuously swept from 0 to 190 Oe (17Hz). New branches of domains appear jumpwise but then practically do not move in  $H_{AC}$  due to the large DW coercivity. Blurred lines over the DS image in the SC area in Fig.12f reveal channels of the enhanced vortex motion forming at high AC fields. Visually, the process of development of the domain structure in the saturated state under increasing AC field is similar to the DC remagnetization presented in Fig.11a-e. One could expect that the refinement of the combined domains in the AC fields should increase the cooperative pinning and decrease the AC losses in the hybrids.

At low temperatures and large amplitudes of the AC field we observed also the appearance of branching TMAs. Similarly to the case of the hybrid with wide domains the TMAs develop at increasing  $H_{AC}$  in the sample with narrow domains at noticeably lower temperatures compared to the Nb film on glass (see Fig.8b-c). This observation confirms that the presence of combined domains effectively suppresses thermo-magnetic avalanches.

### 3. Garnet film with irregular domains at low temperatures.

At room temperature this film has growth induced in-plane anisotropy with two perpendicular [100] easy axes. This results in very wide 180 and 90 degree domains with highly mobile straight domain walls. At decreasing temperature both the anisotropy and domain structure go through a series of transitions. The easy axis starts tilting out from the film plane already at  $\sim 250$ K, however the size of resulting irregular domains with tilted magnetization remains large. At  $\sim 50$  K the magnetization of the film goes through the compensation point. Here the total magnetic moment attains minimum and Fe sublattices go through the spin-flip, which is

well resolved by the abrupt inversion of the magneto-optical contrast during cooling in a small applied magnetic field. With further decreasing  $T$  the total magnetization increases showing a typical paramagnetic behavior (the absence of the low-temperature saturation) due to the dominating contribution of the rare-earth sublattice (Fig. 13). The final domain structure around  $T_c$  of the Nb film consists of irregular patches of narrow stripes intermittent with wider out of plane magnetized patches (Fig.14). The aligned orientation of narrow domains in the patches shows that their easy axis is tilted from the film normal in the direction of domain walls. In addition, there are large and mobile saw-tooth domains (not shown in Fig.14) overlaying narrow domains and homogeneous patches. They reveal a thin layer with the in-plane easy axis in addition to the thicker layer with tilted easy axis. Such low- $T$  separation into layers with different anisotropies is well known for garnet films grown by the liquid phase epitaxy ( see ref's in [55]). Unlike mobile in-plane magnetized regions, domains with a tilted easy axis did not move at 9K in the maximum available AC field of  $\sim 500$  Oe. Details of this domain structure were changed after application and switching off a DC field of 1 kOe normal to the film plane. The sample was magnetized in this field nearly to saturation and new domains were formed on reducing  $H$ . However, the qualitative picture of DS remained the same (Fig.14 b). In contrast to garnet films with perpendicular anisotropy, in this sample we could not implement the saturated state at  $H=0$ . At decreasing field the domains appeared already at large  $H$  and at  $H=0$  there was always a developed domain structure. Such a behavior can be referred to the small domain nucleation energy and relatively large magnetostatic energy.

At low temperatures the domain structure in this garnet film was imaged in the polarized light of its own Faraday effect without using the MOI indicator. When the indicator film was placed on the sample, the domains were not resolved indicating the small stray fields on the top surface of the garnet. This can be a direct consequence of the presence at this surface of the in-plane magnetized layer revealed by the extended in-plane domains. As a result, below  $T_c$  the magnetization process near the Nb film boundary started and proceeded as in a SC layer on a non-magnetic substrate (Fig.15). The magnetic flux concentrated at the Nb edge and then penetrated inside in the shape of balloons, defined by imperfections in the SC film [35, 49, 54].

We compared the flux penetration patterns in the Nb area after application of large DC fields, which changed details of the garnet DS as described above. In a series of runs the sample was warmed above  $T_c$  and  $H_{DC}=1\text{kOe}$  was applied and switched off. Then the sample was zero field cooled and the flux entry was observed in the increasing perpendicular field at  $T < T_c$ . The resulting patterns of the flux penetration were very similar independently of the DS preparation conditions. This confirmed that the vortex motion is defined mostly by defects in the Nb film and is weakly coupled to the FM substrate as could be expected in the presence of the in-plane magnetized layer just below the SC film. However, we found that FM domains still affect the flux dynamics in the Nb area by analyzing differences of images taken at small field variations which show the incremental advancement of the penetration front. A comparison of such differences for various initial DS reveals that the shape of the front, although dominated by the Nb film imperfections, changes after changing the domain structure (Fig.16). The limitation of this effect is consistent with small stray fields and the presence of the in-plane magnetized top layer in the garnet. In this case the vortex flux  $\Phi_0$  is perpendicular to  $\mathbf{M}$  and the vortex/domain coupling  $U_M$  in the surface layer vanishes leaving only smaller coupling with domains in a deeper garnet layer.

Theoretical model

## 1. Domain structure of FM films with perpendicular anisotropy

First we consider basic concepts of the domain structure in FM films with a perpendicular easy axis. Domains appear to reduce the energy of the magnetic stray fields ( $E_F$ ) emanating from the FM layer and the balance of  $E_F$  and the energy of domain walls  $E_{DW}$  establishes the equilibrium domain width. For a lattice of parallel stripe domains of width  $D$  in the film of thickness  $d_F$  the magnetic energy per unit area of the film is presented by the magnetostatic sum:

$$E_F(D) = \sum_{q=\frac{\pi(2k+1)}{D}} (1 - \exp(-qd_F)) \frac{16M^2 D}{\pi^2 (2k+1)^3}$$

where  $M$  is the saturation magnetization and  $k=0,1,2,\dots$ . For  $D \ll d_F$  we obtain the standard result [56]  $E_F = \frac{14}{\pi^2} M^2 D \zeta(3)$  ( $\zeta(3) = 1.202$ ). However, in the limit  $D \gg d_F$ :

$$E_F(D) \approx \sum_k \frac{d_F 16M^2}{\pi(2k+1)^2} - \sum_0^{k_{\max}=D/d_F} \frac{d_F^2}{2D} \frac{16M^2}{(2k+1)} \approx 2\pi M^2 d_F - \frac{4M^2 d_F^2}{D} \ln\left(\frac{D}{d_F}\right) \quad (3)$$

With the domain wall energy density  $\sigma_{DW}$  the total energy per unit area of the film is:

$$E_F + E_{DW} = E_F(D) + \sigma_{DW} \frac{d_F}{D}$$

Minimization of the total energy gives the equilibrium domain width. For  $D \ll d_F$  (narrow domains) we get a traditional square-root dependence describing the monotonic increase of the domain width with the FM film thickness:

$$D = \sqrt{\frac{\sigma_{DW} d_F}{1.7M^2}}$$

However, for  $D \gg d_F$  (wide domains) we obtain a qualitatively different result (see also [57]):

$$D = d_F \exp\left(1 + \frac{\sigma_{DW}}{4M^2 d_F}\right) \quad (4)$$

Here, the domain width diverges exponentially at decreasing  $d_F$ . Such a behavior is expected when the DW energy is large  $\sigma_{DW} > 8M^2 d_F$ . It has a simple physical explanation: the stray fields of wide domains are mainly localized near the domain walls and  $E_F$  is weakly dependent on  $D$ , so that the domain wall energy becomes the dominant factor promoting the expansion of domains.

## 2. Domains in SC/FM hybrid. Total Meissner screening.

When a SC layer much thicker than the penetration depth is placed on the FM film, the stray fields ( $H_s$ ) of the FM domains can be totally screened at the SC/FM interface. In the case of narrow domains,  $D < d_F$ , such a screening will increase twice the density of  $H_s$  near the interface but leave them only in the space below the superconductor. On the other side of the FM film  $H_s$  will stay intact. Then the total magnetostatic energy will increase 1.5 times causing the reduction of the domain width by  $(1.5)^{1/2}$  [42-46]. If the SC film is *thin* and the FM domain width is smaller than the effective London penetration depth  $\lambda_{\text{eff}}$ , the screening is negligible and the domain shrinkage should be small,  $\sim 0.08 (D/\lambda_{\text{eff}})$  of the initial  $D$  [42].

In the case of wide domains,  $D \gg d_F$  and a *thick* SC layer the magnetostatic energy can be estimated as the energy of current strings along the domain walls producing normal fields  $\pm B_z \sim 2d_F M/x$  on two sides of the walls. These currents sustain the circulation from  $+M$  to  $-M$  around DWs. For the infinite penetration depth  $\lambda = \infty$  (no screening) we have a negative magnetostatic contribution per unit area:

$$\delta E_F = -\frac{2}{D} \int MB_z dr \sim -\frac{2}{D} \int_{d_F}^D 2d_F^2 M^2 \frac{dx}{x} \sim -\frac{4M^2 d_F^2}{D} \ln(D/d_F) \quad (5)$$

which naturally reproduces the normal state case (3).

For a finite  $\lambda$  the screening currents around the domain wall will suppress the stray fields at distances  $x > \lambda$ . For  $\lambda \gg D$  the above estimate (5) holds and the domain size should not change compared to the normal state. However, at  $\lambda \ll D$  the result is modified. First, let us take  $d_F \ll \lambda \ll D$ . A proper cut-off in the integral for  $\delta E_F$  yields:

$$\delta E_F \sim -\frac{4M^2 d_F^2}{D} \ln(\lambda/d_F) \quad (6)$$

In this case the negative magnetostatic contribution becomes so small that a domain structure becomes unfavorable ( $D \rightarrow \infty$ ). Formally, one gets the same dependence of  $\delta E_F$  and  $E_{DW}$  on  $D$  and thus no minimum of energy. A critical value of  $\lambda$  favoring the disappearance of domains should be close to the equilibrium domain size in the normal state:

$$\lambda_c \approx d_F \exp\left(\frac{\sigma_{DW}}{4M^2 d_F}\right) \quad (7)$$

Obviously, at  $D \gg d_F$  and  $\lambda \sim d_F$  or  $\lambda \ll d_F$  we are in the limit  $\lambda < \lambda_c$ , the magnetostatic term is negligible, and the domain structure is suppressed.

For SC films of intermediate thickness  $d_S > \lambda$  the results are the same as for the thick SC layer. And for  $d_S \ll \lambda$  above formulas will be also applicable, except  $\lambda$  should be changed for  $\lambda_{\text{eff}} = 2\lambda^2/d_S$ . For example, for  $d_F \ll \lambda_{\text{eff}} \ll D$  we get:

$$\delta E_{MS} \sim -\frac{4M^2 d_F^2}{D} \ln(\lambda_{\text{eff}}/d_F) \quad (8)$$

and the domain structure is suppressed at:

$$2\lambda_c^2/d_s \approx d_F \exp\left(\frac{\sigma_{DW}}{4M^2d_F}\right) \quad (9)$$

Thus, at  $D < d_F$  the superconducting cover layer increases the magnetostatic energy causing some *contraction* of the FM domains. However, at  $D \gg d_F$  the superconducting screening always suppresses the magnetostatic term and should *increase* the *equilibrium* domain size. Similar behavior was numerically predicted in [43].

### 3. Combined domains in SC/FM bilayers. Equilibrium state.

When a SC layer is placed on the FM film with large enough perpendicular magnetization, vortices can spontaneously form above the FM domains if their energy is less than the energy of the domain/vortex coupling [42, 58-60]. For wide domains,  $D > d_F$ , in a thin FM film the appropriate condition is  $\epsilon_0 d_s < M\Phi_0 d_F$  [59], where  $\epsilon_0$  is the unit vortex line energy. In the condition for narrow domains  $D$  substitutes for  $d_F$ :  $\epsilon_0 d_s < 0.37M\Phi_0 D$  [60-61]. And for very thin SC films, when the effective penetration depth is larger than the domain width,  $\lambda_{\text{eff}} \gg D$ , it becomes  $\epsilon_0 d_s (\lambda_{\text{eff}}/D) < 5.4 \times 10^{-3} M\Phi_0 D$  [42].

Now we consider a situation when the condition for the vortex formation is fulfilled, so that the SC/FM bilayer carries  $n_v(x)$  density of vortices of proper polarity in each domain. Domains in the thin FM film are wide,  $D \gg d_F$ , and  $d_s \ll D$ . The total energy of the system will be the energy of individual vortices ( $E_v$ ) including the energy of their coupling to magnetic domains, energy of vortex-vortex interactions ( $E_{v-v}$ ), energy of FM domain walls ( $E_{DW}$ ), and magnetostatic energy ( $E_F$ ). Following calculations in [62], the vortex density obtained from minimization of  $E_v + E_{v-v}$  with a corrected coefficients for the single vortex energy,  $\epsilon_v = \epsilon_0 d_s - M\Phi_0 d_F$ , can be presented as:

$$n_v(x) = -\frac{4\pi\epsilon_v}{\Phi_0^2 D} \frac{1}{\sin\frac{\pi x}{D}} \quad (10)$$

Direct integration of  $n_v(x)$  yields the total number of vortices per unit length of a stripe domain:

$$N_v \approx \frac{8d_F(M - \epsilon_0 d_s / (\Phi_0 d_F))}{\Phi_0} \ln \frac{D}{d_F} \quad (11)$$

Eq. (11) shows that the equilibrium number of vortices in domains is in a direct correspondence with the domain width. This relation turns out to be very strong because  $D$  is exponentially dependent on  $N_v$ . We will use this fact later discussing possible instabilities in the combined domain structure.

Using the approach of [62] we obtain the total energy  $E_{DW} + E_v + E_{v-v}$  as:

$$E_{\text{tot}} \approx \left( \frac{\sigma_{DW} d_F}{D} - d_F^2 \frac{4(M - \epsilon_0 d_s / (\Phi_0 d_F))^2}{D} \ln \frac{D}{d_F} \right) A_x A_y \quad (12)$$

Here  $A_y$  and  $A_x$  are the in-plane sample dimensions along and perpendicular to the DWs respectively. Stray fields in the hybrid are concentrated near domain walls and screened by the superconductor at distances  $\sim \lambda_{\text{eff}}$  from DWs. Such a confinement produces the magnetostatic energy  $E_F$  scaled with the length of DWs,  $E_F \sim -M^2 d_F^2 A_x A_y / D$ , which decreases the effective energy of domain walls. However, we can neglect this contribution compared to  $E_{\text{DW}} = \sigma_{\text{DW}} d_F A_x A_y / D$  accounting that for wide domains  $\sigma_{\text{DW}} \gg M^2 d_F$ . From the minimum of  $E_{\text{tot}}$  the equilibrium domain width is obtained as:

$$D_{\text{eq}} = d_F \exp \left( 1 + \frac{\sigma_{\text{DW}}}{4(M - \varepsilon_0 d_s / (\Phi_0 d_F)^2 d_F)} \right) \quad (13)$$

This expression (compare with (4)) describes the renormalization of the magnetic energy due to the coupling of vortices and magnetic domains. It shows that in the presence of vortices in the SC layer the equilibrium domains should expand compared to the normal state. To sum up, in both Meissner and vortex states a thin superconducting film suppresses the FM domain structure resulting in the *increase* of the domain width.

#### 4. Combined domains in SC/FM bilayers. Nonequilibrium state. Fixed number of vortices.

Eq.7a shows that in wide domains the density of vortices  $n_v$  increases towards the domain walls. It changes from maximum positive to the maximum negative density across the DW. In the equilibrium state the SC layer carries the depairing current along the DW, which supports the largest possible gradient of  $n_v$  across the wall. If the number of vortices in the domains is reduced below the equilibrium number  $N_{\text{eq}}$ , the current along the domain wall drops below the depairing value and vortices become locked in the domain. This corresponds to the case with a fixed number of vortices bounded by the potential barriers due to the domain wall currents. Now we should find the minimum of the energy functional under the condition of  $N = \text{const}$ . This functional will have the same form as in [62] but instead of the standard factor  $-M\Phi_0 d_F + \varepsilon_0 d_s$  in the single vortex energy we will use a Lagrange coefficient, which can be conveniently written as  $-\tilde{M}\Phi_0$ :

$$E_v^{\text{tot}}(N = \text{const}) = -\tilde{M}\Phi_0 d_F \int n(\vec{r}) s(\vec{r}) d\vec{r} + \frac{1}{2} \int n(\vec{r}') V(\vec{r} - \vec{r}') n(\vec{r}) d\vec{r} d\vec{r}' \quad (14)$$

Here, following the notations of [62]  $s(\mathbf{r})$  is a periodic step function equal +1 and -1 in neighboring domains and  $V(\vec{r} - \vec{r}') = \Phi_0^2 / (4\pi |\vec{r} - \vec{r}'|)$  is the Pearl's vortex interaction potential.

From the minimization of (11a) we obtain the same results as in the previous section but with  $\tilde{M}$  instead of  $M - \varepsilon_0 d_s / (\Phi_0 d_F)$ . The fixed number of vortices per unit length of the stripe domain is now:

$$N \approx \frac{8d_F \tilde{M}}{\Phi_0} \ln \frac{D}{d_F} = \text{const} \quad (15)$$

And the total energy can be presented as:

$$E = (d_F \frac{\sigma_{DW}}{D} - \frac{N^2 \Phi_0^2}{16D \ln \frac{D}{d_F}}) A_x A_y \quad (16)$$

This energy is positive for large D and reaches maximum at:

$$D_{\max} = d_F \exp(1 + N^2 \Phi_0^2 / 16 d_F \sigma_{DW}) \quad (17)$$

At decreasing the domain width the nonequilibrium E changes sign. The energy drops at decreasing D below  $D_{\max}$ , which means that the system becomes unstable with respect to the contraction of domains. During the domain contraction with a fixed number of vortices, the gradient of the vortex density near the domain walls increases until the current along DWs acquires the depairing value. From this moment the system returns to the equilibrium regime: vortices and antivortices enter near the domain walls and domains expand towards the equilibrium width (13). The whole process is illustrated in Fig.17. Calculating the crossing point for E(D) curves (12) and (16) we can find the size  $D^*$  when the system returns to the equilibrium regime:

$$D^* = d_F \exp\left(\frac{N_{ne} \Phi_0}{8d_F (M - \varepsilon_0 d_S / (\Phi_0 d_F))}\right) \quad (18)$$

Below we give an estimate of  $D^*$  and compare it with  $D_{\text{eq}}$ .

##### 5. Effect of the AC field on the combined domain structure.

The above calculations do not explicitly account for the pinning dependent flux dynamics. However, they allow us to pinpoint the main mechanism of the observed domain shrinkage in the AC field. Upon cooling through  $T_C$  in the absence of  $H_{AC}$  an equilibrium number of vortices and antivortices will be created in neighboring domains. Close to  $T_C$  the domain size is practically the same as in the normal state due to the small  $\varepsilon_0$  and  $d_S/d_F \ll 1$  in (13). At further decreasing temperature  $\varepsilon_0$  will increase. So the equilibrium number of vortices in domains should decrease (see (11)) and domains should expand (see (13)). However, pinning can delay this process. In the presence of  $H_{AC}$ , the domain walls oscillate causing a partial vortex-antivortex annihilation around them. As a result the number of vortices in domains is reduced below  $N_{\text{eq}}$  and the evolution of the domain width switches to the nonequilibrium route (dashed curve in Fig.17) so that the domains shrink to  $D=D^*$ . If there were a sufficient supply of vortices which would allow an increase of their density in the domains (e.g. vortex creep from the edge at larger T), the system could return to the equilibrium state and domains would expand from  $D^*$  to  $D_{\text{eq}}$ . However, if the vortex supply is delayed (due to the pinning at lower T), the observed domain width can remain at  $D^*$ . We estimate  $D^*$  by taking  $D_{\max} \sim D_{\text{eq}}$ , which yields  $N_{ne} = \sigma_{DW} / (M - \varepsilon_0 d_S / (\Phi_0 d_F)) \Phi_0$  so that

$$D^* = d_F \exp\left(\frac{\sigma_{DW}}{4d_F (M - \varepsilon_0 d_S / (\Phi_0 d_F))^2}\right) = D_{\text{eq}} / e \quad (19)$$

This estimate agrees remarkably well with the maximum shrinkage of  $\sim 3$  times observed in the sample with wide domains at lowest temperatures. The described scenario explains also the negligible changes of the domain width in the hybrid at larger temperatures, when the fast flux relaxation restores the equilibrium. Moreover, it clarifies why the domains are wider near the edge of the SC film and narrower at the AC field penetration front. Close to the edge,  $H_{AC}$  provides a better supply of vortices and here the situation is closer to equilibrium. However, further inside the SC the vortex supply is reduced due to pinning and the nonequilibrium state forms easier yielding the smallest domains at the largest depth of the field penetration.

To confirm that the reduced vortex density is the reason for the domain contraction we plotted the intensity profiles of the magneto-optical images across wide and narrow domains in the hybrid area as illustrated in Fig.18. These intensity profiles correspond to  $B_z(x)$  plots, i.e. the vortex density distributions across the domains. They clearly show that in the wide combined domains the vortex density is on the average larger compared to the shrunk domains. Also  $B_z$  in the wide domains increases towards the domain walls while it smoothly decays near the DWs of shrunk domains. Such a behavior shows that there is a large current along the boundaries of wide domains and it is small along the DWs of the squeezed domains. This is in direct agreement with the proposed model.

## Conclusions

In this work we experimentally observed and theoretically calculated a unique type of domains in superconducting/ferromagnetic bilayers. Strong coupling between vortices in the SC film and magnetization in FM films with perpendicular anisotropy results in a combined domain structure where vortices reside on top of magnetic domains of the same polarity. The presence of such combined domains modifies the electromagnetic response of the hybrid and essentially decelerates the magnetic flux dynamics. Unlike in usual type-II superconductors, where the magnetization process occurs through the entry and exit of vortices, in our hybrids the magnetization goes on through the expansion and contraction of combined domains as in type-I superconductors. The remaining domains polarized against the applied field serve as a vortex drain network when the field is decreased. The synergetic action of the vortex pinning in the superconductor, pinning of the domain walls in the magnetic layer, and the pinning of vortices by the magnetic domain walls provides a strong cooperative pinning, which arrests the flux motion and efficiently suppresses thermo-magnetic avalanches. In equilibrium the combined domains with  $D \gg d_F$  should expand beyond the normal domain width. However, if the density of vortices in the domains is reduced below the equilibrium value, the same coupling between vortices and magnetization causes a new type of dynamic instability. It results in a strong contraction of combined domains down to  $\sim 1/3$  of their equilibrium width. We observe such a behavior in large enough AC fields causing vortex-antivortex annihilation near oscillating domain walls and decreasing the vortex density in the domains. In a sample with narrow stripe domains the cooperative pinning also results in a substantial attenuation of the flux dynamics. Here the domain width practically does not vary in AC fields but moving vortices align the domain walls parallel to the direction of their motion. This effect is reciprocal to the guidance of vortices by magnetic domain walls that we observed earlier [30-31].

We believe that the magnetic pinning offered by the combined domain structures can expand the working temperature range of high- $T_c$  superconductors suffering from the enhanced vortex dynamics close to the transition temperature. Appropriate experiments are on the way.

## Acknowledgements

The submitted manuscript has been created by UChicago Argonne, LLC, Operator of Argonne National Laboratory (“Argonne”). Argonne, a U.S. Department of Energy Office of Science Laboratory, is operated under Contract No. DE-AC02-06CH11357.

## References

- [1] S. S. Saxena, P. Agarwal, K. Ahilan, F. M. Grosche, R. K. W. Haselwimmer, M. J. Steiner, E. Pugh, I. R. Walker, S. R. Julian, P. Monthoux, G. G. Lonzarich, A. Huxley, I. Sheikin, D. Braithwaite, J. Flouquet, *Nature* **406**, 587 (2000).
- [2] A. I. Buzdin, M. Y. Kuprianov, *Pis'ma Zh. Eksp. Teor. Fiz.* **52**, 1089 (1990) [*JETP Lett.* **52**, 487 (1990)].
- [3] J. S. Jiang, D. Davidovic, D. H. Reich, and C. L. Chien, *Phys. Rev. Lett.* **74**, 314 (1995).
- [4] J. Y. Gu, C. -Y. You, J. S. Jiang, J. Pearson, Ya. B. Basaliy, S. D. Bader, *Phys. Rev. Lett.* **89**, 267001 (2002). Fine scale modulations of the order parameter:
- [5] P. Fulde and R. A. Ferrell, *Phys. Rev. A* **135**, 550 (1964).
- [6] A. I. Larkin, Y. N. Ovchinnikov, *Zh. Eksp. Teor. Fiz.* **47**, 1136 (1964) [*Sov. Phys. JETP* **20**, 762 (1965)].
- [7] P. W. Anderson and H. Suhl, *Phys. Rev.* **116**, 898 (1959).
- [8] V. A. Oboznov, V. V. Bol'ginov, A. K. Feofanov, V. V. Ryazanov, and A. I. Buzdin, *Phys. Rev. Lett.* **96**, 197003 (2006).
- [9] A. F. Volkov, F. S. Bergeret, K. B. Efetov, *Phys. Rev. Lett.* **90**, 117006 (2003).
- [10] T. S. Khaire, M. A. Khasawneh, W. P. Pratt, N. O. Birge, *Phys. Rev. Lett.* **104**, 137002 (2010).
- [11] J. W. Robinson, J. D. S. Witt, M. G. Blamire, *Science* **329**, 59 (2010).
- [12] A. Yu. Aladyshkin and V. V. Moshchalkov, *Phys. Rev. B* **74**, 064503 (2006).
- [13] L. N. Bulaevskii, E. M. Chudnovsky, and M.P. Maley, *Appl. Phys. Lett.* **76**, 2594 (2000)
- [14] J. I. Martin, M. Velez, J. Nogues, I.K. Schuller, *Phys. Rev. Lett.* **79**, 1929 (1997).
- [15] Y. A. Izyumov, Y. N. Proshin, and M. G. Khusainov, *Phys. Usp.* **45**, 109 (2002).
- [16] A. I. Buzdin, *Rev. Mod. Phys.* **77**, 935 (2005).
- [17] I. F. Lyuksyutov, V. L. Pokrovsky, *Adv. Phys.* **54**, 67 (2005).
- [18] F. S. Bergeret, A. F. Volkov, K. B. Efetov, *Rev. Mod. Phys.* **77**, 1321 (2007).
- [19] M. Velez, J. I. Martin, J. E. Villegas, A. Hoffmann, E. M. Gonzalez, J. L. Vicent, I. K. Schuller, *J. Mag. Magn. Mat.* **320**, 2574 (2008).
- [20] A. Yu. Aladyshkin, A. V. Silhanek, W. Gillijns, V. V. Moshchalkov, *Superc. Sci. Technol.* **22**, 053001 (2009).
- [21] A. M. Campbell, J. E. Evetts, *Adv. Phys.* **21**, 199 (1972).
- [22] S. R. Foltyn, L. Civale, J. L. Macmanus-Driscoll, Q. X. Jia, B. Maiorov, H. Wang, M. Maley, *Nat. Mater.* **6**, 631 (2007).
- [23] B. Maiorov, S. A. Baily, H. Zhou, O. Ugurlu, J. A. Kennison, P. C. Dowden, T. G. Holesinger, S. R. Foltyn, L. Civale, *Nat. Mater.* **8**, 398 (2009).
- [24] I. F. Lyuksyutov, *J. Supercond. Nov. Magn.* **23**, 1047 (2010).
- [25] K. Kim, I. Lyuksyutov, D. G. Naugle, *Superc. Sci. Technol.* **24**, 024013 (2011).
- [26] M. Lange, M. J. Van Bael, V. V. Moshchalkov, Y. Bruynseraede, *Appl. Phys. Lett.* **81**, 322 (2002).
- [27] D. B. Jan, J. Y. Coulter, M. E. Hawley, L. N. Bulaevskii, M. P. Maley, Q. X. Jia, B. B. Maranville, F. Hellman, X. Q. Pan, *Appl. Phys. Lett.* **82**, 778 (2003).

- [28] M. Lange, M. J. Van Bael, V. V. Moshchalkov, *Physica C* **408**, 522 (2004).
- [29] M. Z. Cieplak, X. M. Cheng, C. L. Chien, H. Sang, *J. Appl. Phys.* **97**, 026105 (2005).
- [30] V. Vlasko-Vlasov, U. Welp, G. Karapetrov, V. Novosad, D. Rosenmann, M. Iavarone, A. Belkin, W.-K. Kwok, *Phys. Rev. B* **77**, 134518 (2008).
- [31] V. K. Vlasko-Vlasov, U. Welp, A. Imre, D. Rosenmann, J. Pearson, W. K. Kwok, *Phys. Rev. B* **78**, 214511 (2008).
- [32] V. Vlasko-Vlasov, U. Welp, W. Kwok, D. Rosenmann, H. Claus, A. A. Buzdin, and A. Melnikov, *Phys. Rev. B* **82**, 100502 (2010).
- [33] L. Y. Zhu, M. Z. Cieplak, C. I. Chien, *Phys. Rev. B* **82**, 060503 (2010).
- [34] K. H. J. Buschow, *Concize encyclopedia of magnetic and superconducting materials*, Elsevier, 2005.
- [35] V. K. Vlasko-Vlasov, U. Welp, G. W. Crabtree, and V. I. Nikitenko, in *Physics and Materials Science of Vortex States, Flux Pinning and Dynamics*, edited by R. Kossowsky S. Bose, V. Pan, and Z. Durusoy, NATO Advanced Studies Institute, Series E: Applied Science Kluwer, Dordrecht, 1999, Vol. 356, p. 205.
- [36] M. Reibelt, A. Schilling, N. Toyota, *Phys. Rev. B* **81**, 094510 (2010).
- [37] Z. Malek, V. Kambarsky, *Czech. J. Phys.* **8**, 416 (1958).
- [38] C. Kooy, U. Enz, *Philips Res. Rep.* **15**, 7 (1960).
- [39] T. G. W. Blake, C. C. Shir, Y. O. Tu, E. DellaTorre, *IEEE Trans. Magn.* **18**, 985 (1982).
- [40] T. Tamegai, Y. Nakao, Y. Nakajima, *J. Phys.: Conf. Ser.* **150**, 152263 (2009).
- [41] T. Tamegai, Y. Nakao, S. Mohan, Y. Nakajima, *Supercond. Sci. Technol.* **24**, 024015 (2011).
- [42] G. M. Genkin, V. V. Skuzovatkin, L. D. Tokman, *J. Magn. Magn. Mater.* **130**, 51 (1994).
- [43] A. Stankiewicz, S. J. Robinson, G. A. Gehring, V. V. Tarasenko, *J. Phys: Cond. Mat.* **9**, 1019 (1997).
- [44] L. N. Bulaevskii, E. M. Chudnovsky, *Phys. Rev. B* **63**, 012502 (2000).
- [45] E. B. Sonin, *Phys. Rev. B* **66**, 136501 (2002).
- [46] L. N. Bulaevskii, E. M. Chudnovsky, M. Daumens, *Phys. Rev. B* **66**, 136502 (2002).
- [47] E.H.Brandt, M.V. Indenbom, *Phys. Rev. B* **48**, 12893 (1993).
- [48] E. Zeldov, J.R. Clem, M. McElfresh, M. Darwin, *Phys. Rev. B* **49**, 9802 (1994).
- [49] V. K. Vlasko-Vlasov, U. Welp, V. Metlushko, and G. W. Crabtree, *Phys. Rev. B* **69**, 140504R (2004).
- [50] R.G. Mintz, A.L. Rakhmanov, *Rev. Mod. Phys.* **53**, 551 (1981).
- [51] P. Leiderer, J. Boneberg, P.Brull, V. Bujok, S. Herminghaus *Phys. Rev. Lett.* **71**, 2646 (1993).
- [52] E. Altshuler, T.H. Johansen, *Rev. Mod. Phys.* **76**, 471 (2004).
- [53] I. S. Aranson, A. Gurevich, M. S. Welling, R. J. Wijngaarden, V. K. Vlasko-Vlasov, V. M. Vinokur, U. Welp, *Phys. Rev. Lett.* **94**, 037002 (2005).
- [54] A. Gurevich, M. Friesen, *Phys. Rev. B* **62**, 4007 (2000).
- [55] I. E. Dikshstein, F. V. Lisovskii, C. M. Park, *J. Magn. Magn. Mat.* **167**, 34 (1997).
- [56] L.D. Landau, E.M. Lifshitz, *Electrodynamics of Continuous Media*, Pergamon, Oxford (1984).
- [57] B. Kaplan and G. A. Gehring, *J. Magn. Magn. Mater.* **128**, 111 (1993).
- [58] E.B.Sonin, *Pis'ma Zh. Tekh. Fiz.* **14**, 1640 (1988), {*Sov. Tech. Phys. Lett.* **14**, 714 (1988)}.
- [59] I. F. Lyuksyutov, V. L. Pokrovsky, *Mod. Phys. Lett.* **B14**, 409 (2000).
- [60] Yu.I.Bespyatykh, W.Wasilevski, *Phys. Sol. State* **43**, 224 (2001), {*Fizika Tverdogo Tela* **43**, 215 (2001)}.

- [61] R. Laiho, E. Landeranta, E.B. Sonin, K.B. Traito, Phys. Rev. B **67**, 144522 (2003).  
[62] S. Erdin, I.F. Lyuksyutov, V.L. Pokrovsky, V.M. Vinokur, Phys. Rev. Lett. **88**, 017001 (2002).

## Figure captions

Fig.1 Magnetization loops of the garnet film with wide domains in the perpendicular- (a) and in-plane –(b) fields at temperatures indicated in the figures. At temperatures below 30K the signal becomes noisy due to the strongly increased paramagnetic substrate contribution.

Fig.2 Temperature dependence of the saturation magnetization for the garnet film with wide domains constructed using  $M(H)$  data in perpendicular fields.

Fig.3 Temperature variations of the domain width  $D$  in the garnet film with wide domains. (a)-magneto-optical pictures of domains at different  $T$ . (b)  $D(T)$  dependence. The insert shows the width of domains in the bare garnet and Nb/garnet areas of the sample after the AC equilibration as described in the text. Results of several cooling runs are shown by different colors.

Fig.4 AC equilibrated domain structure at  $T < T_c$  near the boundary of the Nb covered garnet film with wide domains. The boundary between the bare garnet film (on the left) and Nb covered area (on the right) is shown by white line.

Fig.5 DC remagnetization of the sample with wide domains in the perpendicular field at 6.2K. The Nb film is on the right from black line shown in (a). Values of increasing (a)-(e) and decreasing (g)-(h) fields are shown in the panels. The remagnetization proceeds through the expansion and contraction of appropriate coupled domains.

Fig.6 Remagnetization of the sample with wide domains at 6.2K when the garnet film is saturated (compare with Fig.5). The field increased (a)-(d) to a maximum of 800 Oe (not shown) and then decreased to 0 in the absence of domains showing a traditional exit of vortices near the Nb edge (e)-(f). Successive increase of negative field nucleates domains, which abruptly expand leaving narrow unfavorable domains (white lines in (h)). Reduction of field after saturation in -800 Oe yields the trapped flux pattern (i) similar to (f). Nucleation of domains in a positive field (j) and then decreasing  $H$  restores the combined domain remagnetization scenario.

Fig.7 DC remagnetization of the sample with wide domains at 4.5K. The process in the increasing  $H$ , (a)-(d), is qualitatively similar to that at larger  $T$  (Fig.5-6). However, the vortex pinning is increased and chaotically shooting thermo-magnetic avalanches appear at reducing field from the saturated state (irregular dark and bright lines on the right of figs. (e)-(h)).

Fig.8 Arrest of the thermo-magnetic avalanches appearing in the AC field in the hybrid samples with wide (a) and narrow (b) domains compared to the same Nb film deposited on glass (c).

Fig.9 (a)-  $M(H)$  loops in the perpendicular field, (b) – temperature dependence of the saturation magnetization  $4\pi M_s$  (T), and (c) –in-plane magnetization curves for the sample with narrow domains.

Fig.10 DC magnetization of the sample with narrow domains at 4.5K. Wight line shows the boundary between the bare garnet (right) and Nb covered (left) areas. Values of H are shown on the pictures.

Fig.11 DC remagnetization of the sample with narrow domains at decreasing, (a)-(b), and changing polarity of the field, (c)-(f), after saturation in  $H=+600$  Oe.  $T=4.5$ K. Fields are shown in the left top corners of the pictures.

Fig.12 Development of the combined domain structure in an applied AC field. The initial partially saturated state (a) is obtained after removal of  $H_{DC}=500$  Oe at 4.5K. 17 Hz AC field is applied perpendicular to the film surface. The amplitude is increasing from 0 to 8.8, 19.8, 48, 120, and 190 Oe in panels (a) to (f) respectively. After jump-wise appearance of new domains they remain practically immobile in the AC field ((b) - (e)). Some oscillations of domains appear at large field amplitudes in the Nb area near channels of the enhanced vortex dynamics (blurred lines on the left in (f)).

Fig.13 Temperature dependence of the saturation magnetization in the Tb-garnet film.

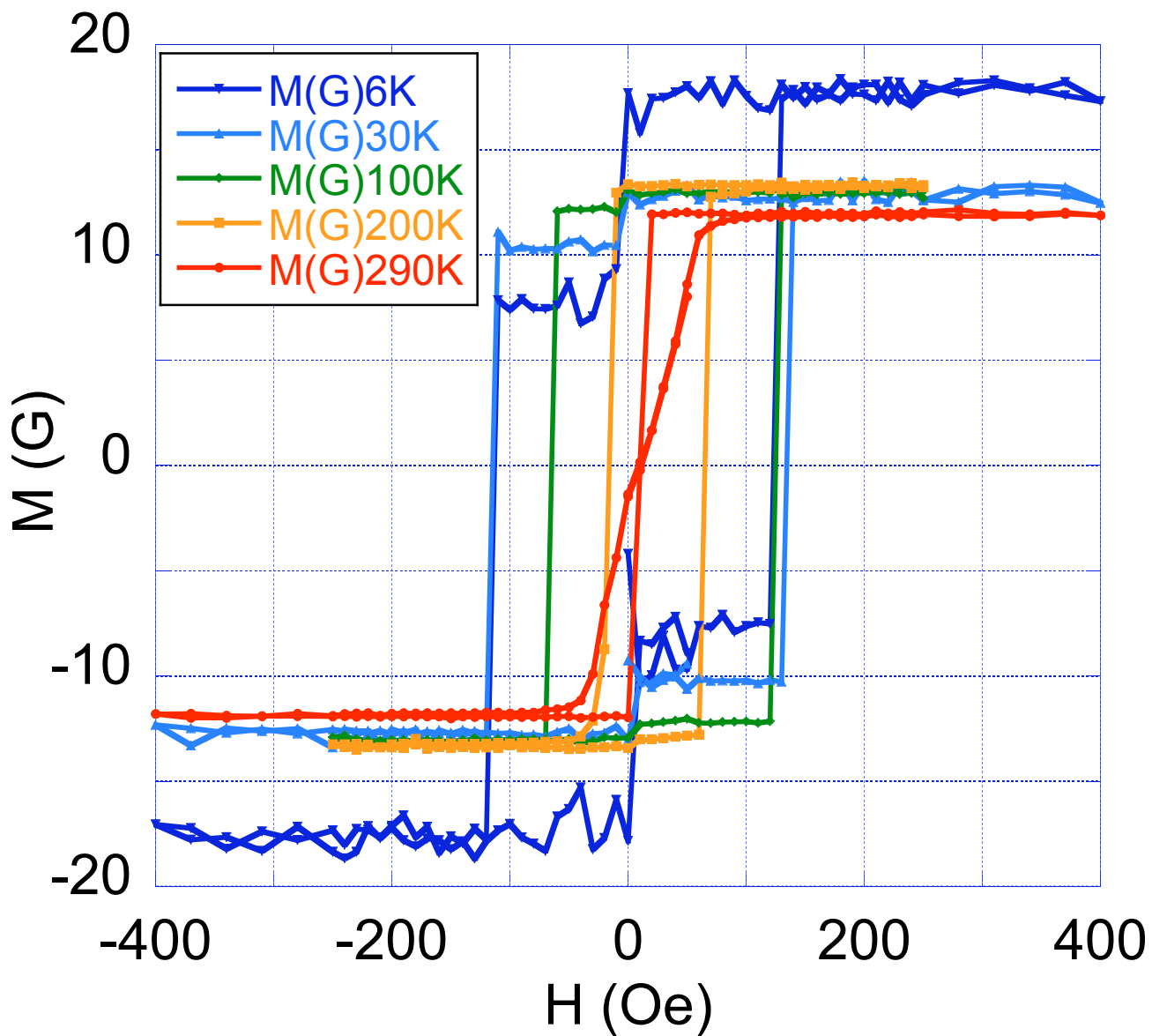
Fig.14 Domain structure in the Tb-garnet film at 9K. (a) and (b) show the same place in the sample before and after application and removal of a perpendicular field of 1 kOe.

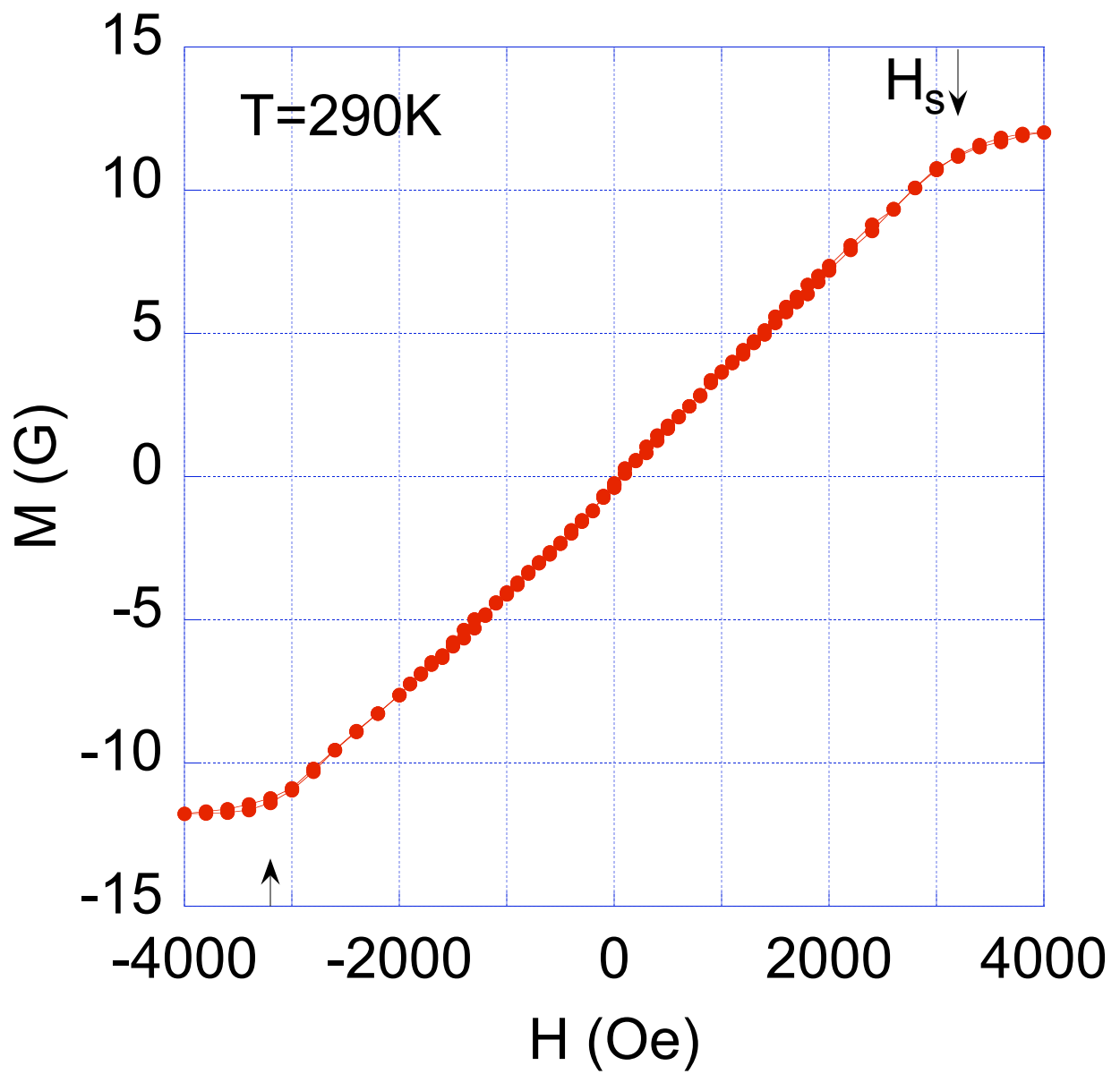
Fig.15 Flux penetration (bright color) from the edge of the Nb film (black line in (a)) deposited on the Tb-garnet.  $T=4.4$ K. Values of the increasing normal field are shown on the pictures.

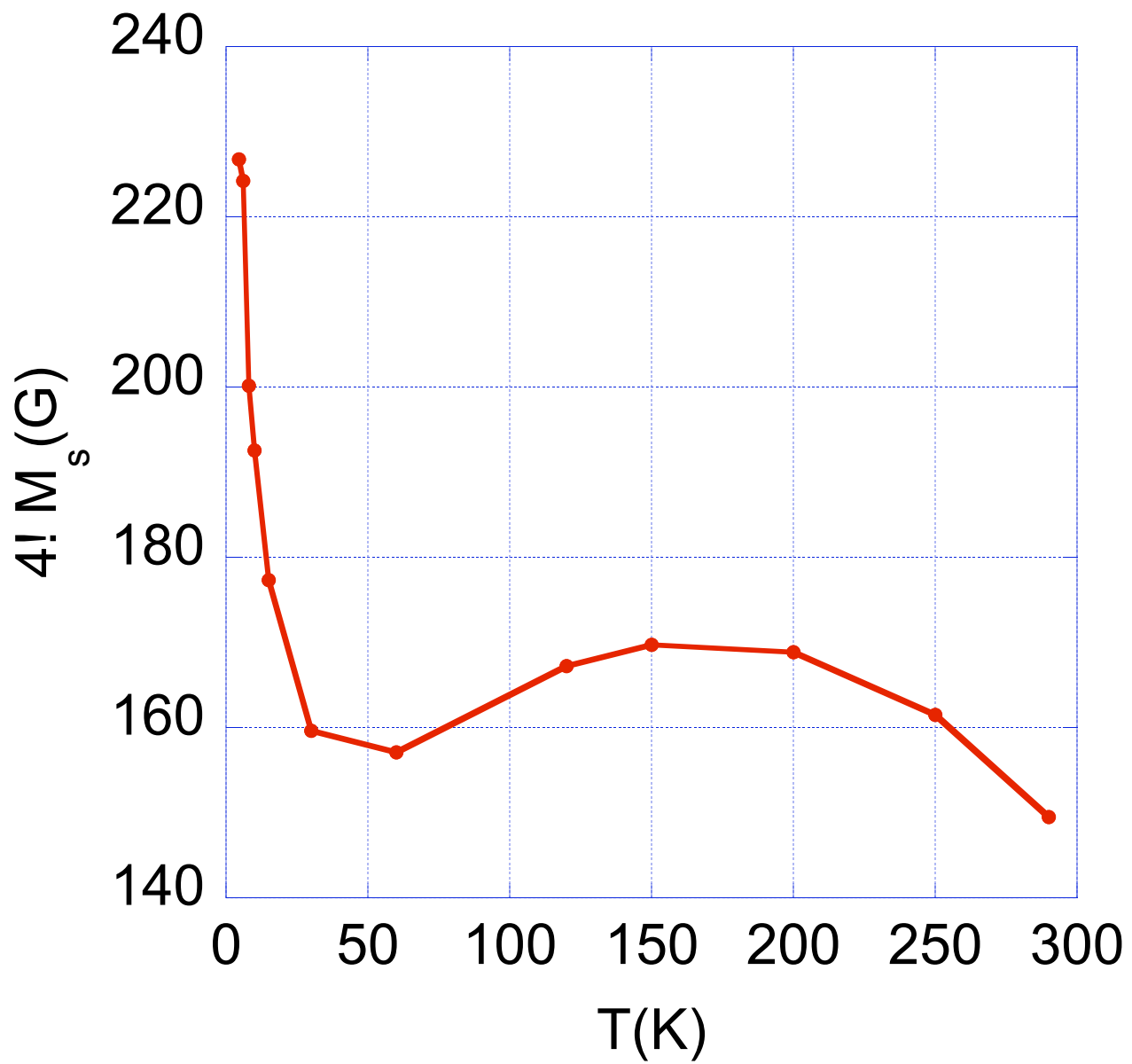
Fig.16 Differences of flux images showing the advancement of the vortex penetration front at 4.4K upon increasing field from 0 to 5.5 Oe. (a) and (b) are obtained in the same conditions but with different domain structures in the Tb-garnet changed as shown in Fig.14. A close similarity and modest variations of the patterns (front shape and depth of penetration) show the domination of the pinning by defects in the Nb film.

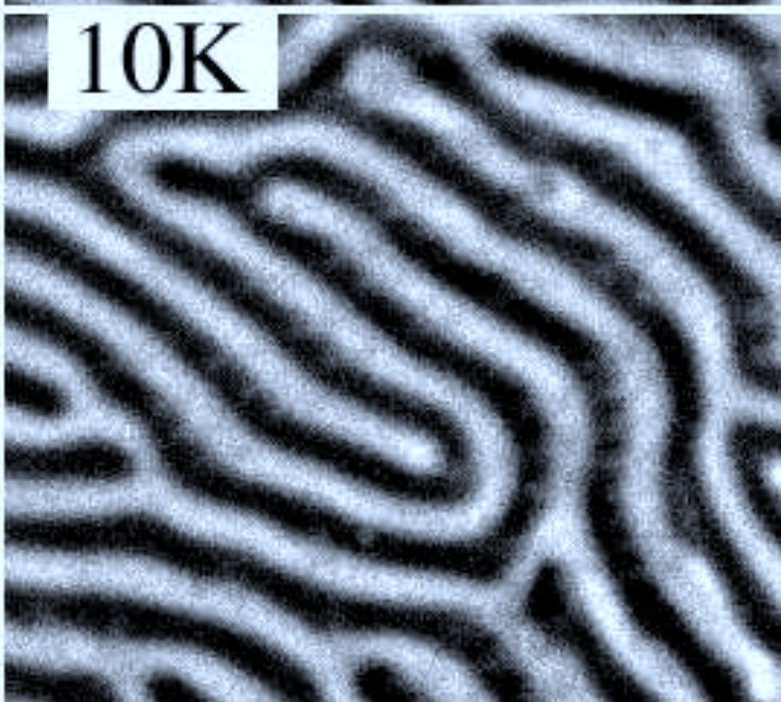
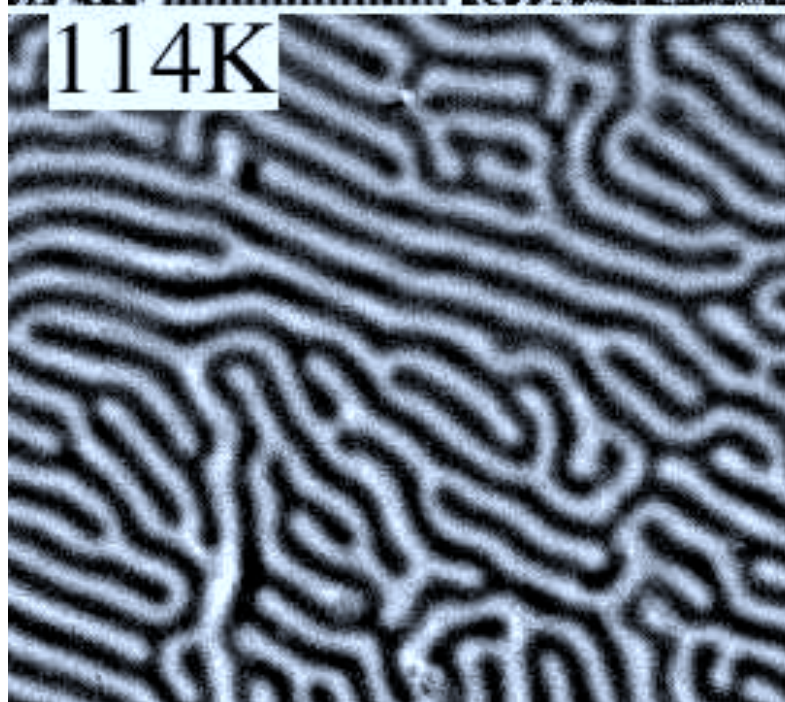
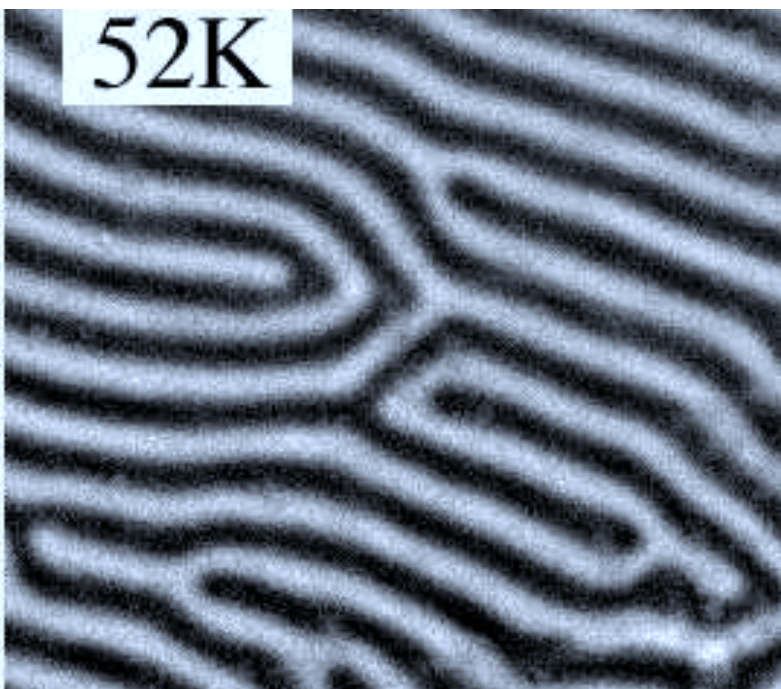
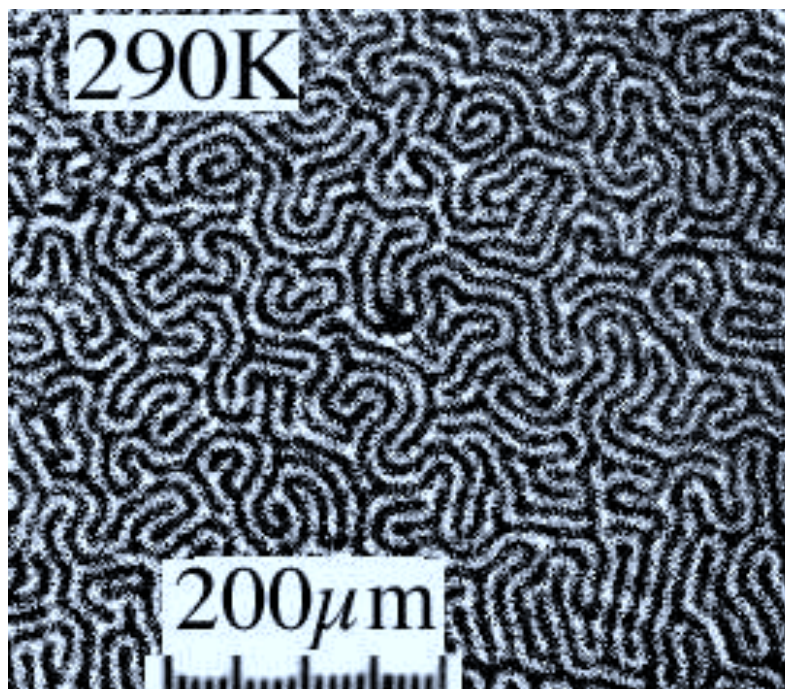
Fig.17 Energy  $E$  of combined domains as a function of their width  $D$ . Solid (red) line corresponds to Eq.12 for the tunable number of vortices in domains with the parameter  $4d_F(M - \epsilon_0 d_s / \Phi_0 d_F)^2 / \sigma_{DW} = 0.3$ . Dashed (black) line corresponds to Eq.16 for the constant number of vortices in domains with the parameter  $N^2 \Phi_0^2 / 16d_F \sigma_{DW} = 3.8$ .

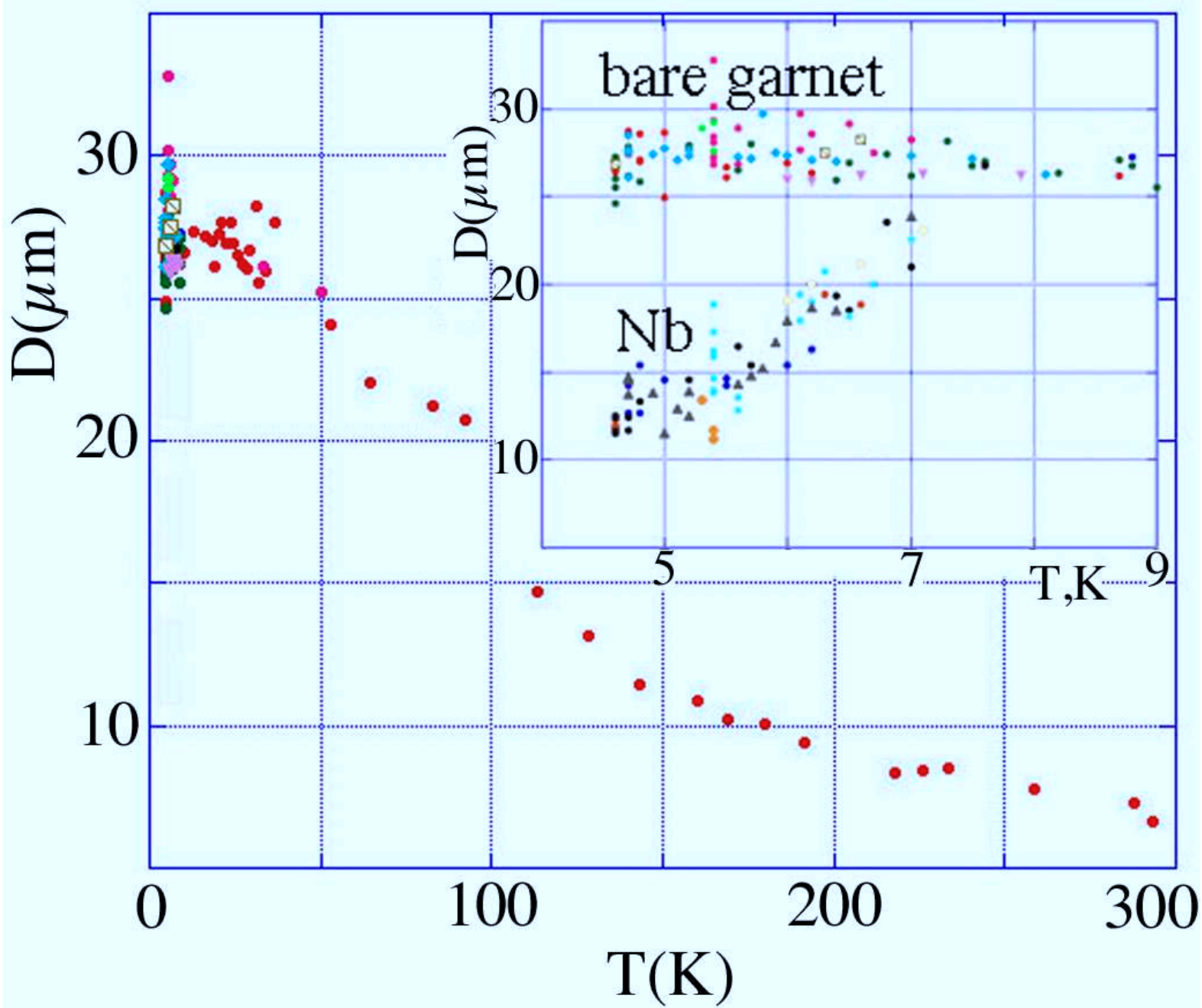
Fig.18 MOI image of combined domains at 5K after application of  $H_{AC}(17 \text{ Hz})=90$  Oe and intensity profiles (inserts) revealing variations of  $B_z$  across the domains. Profiles are measured in rectangles outlined by white lines. SC area is below the line marking the Nb edge. Average  $B_z$  is larger in wide domains and increases towards DWs.  $B_z$  is smaller and smoothly decays towards DWs in shrunk domains.

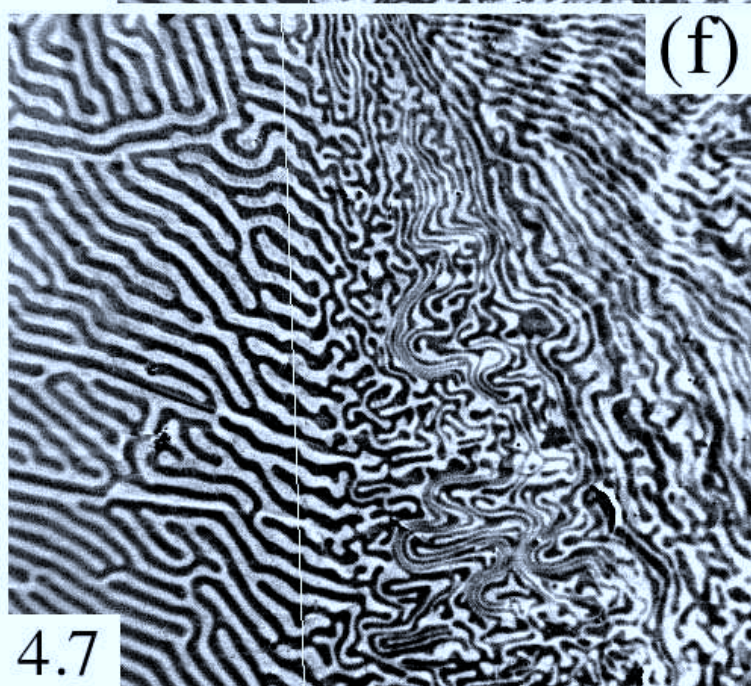
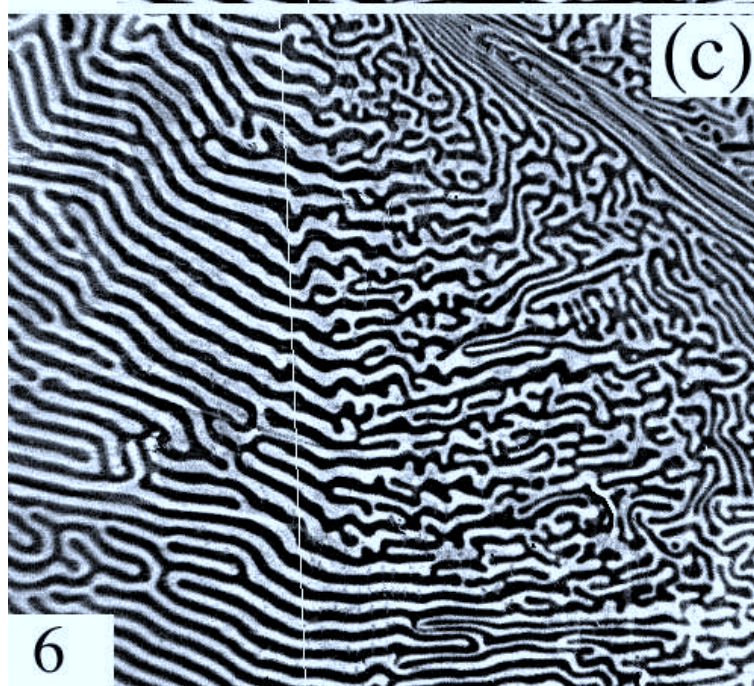
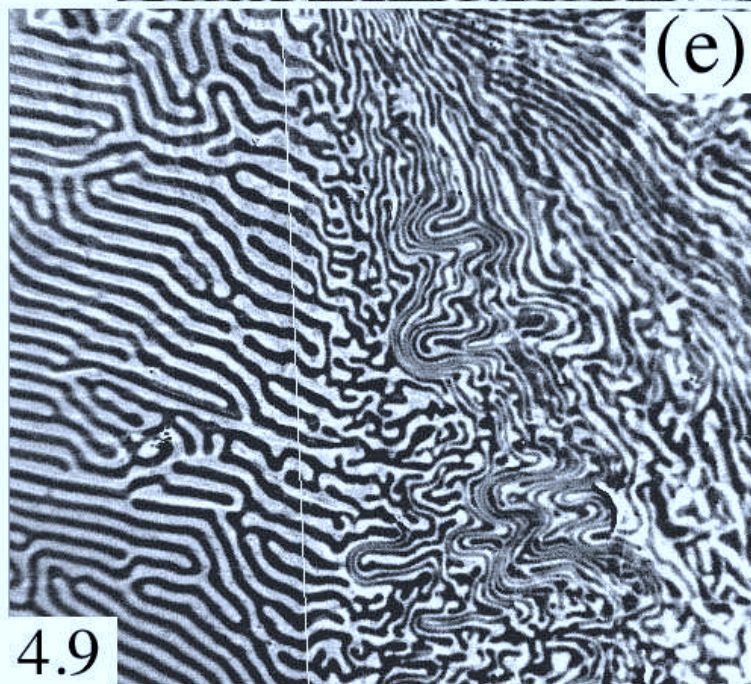
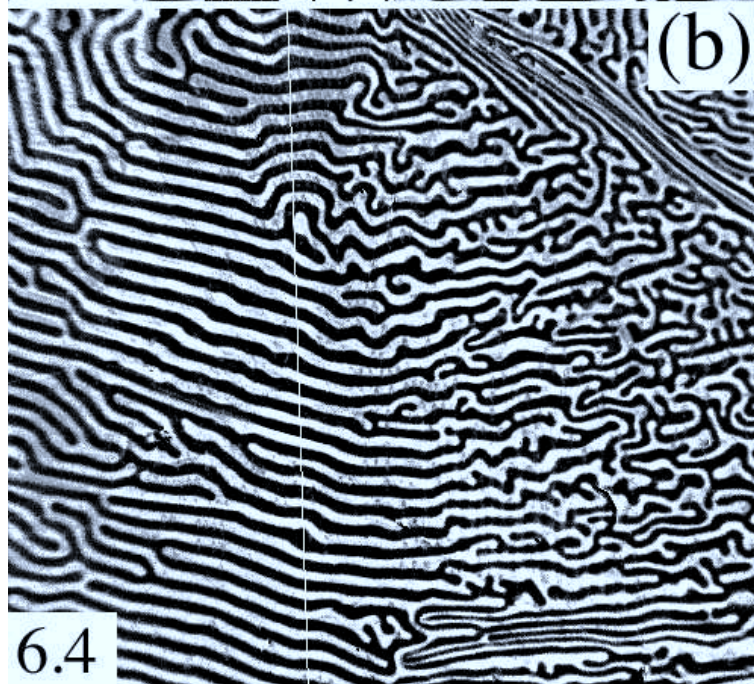
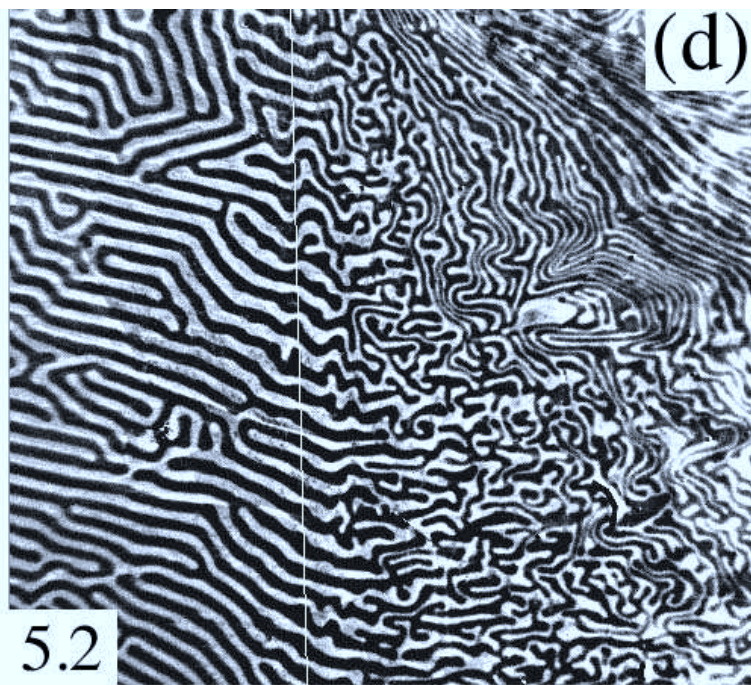
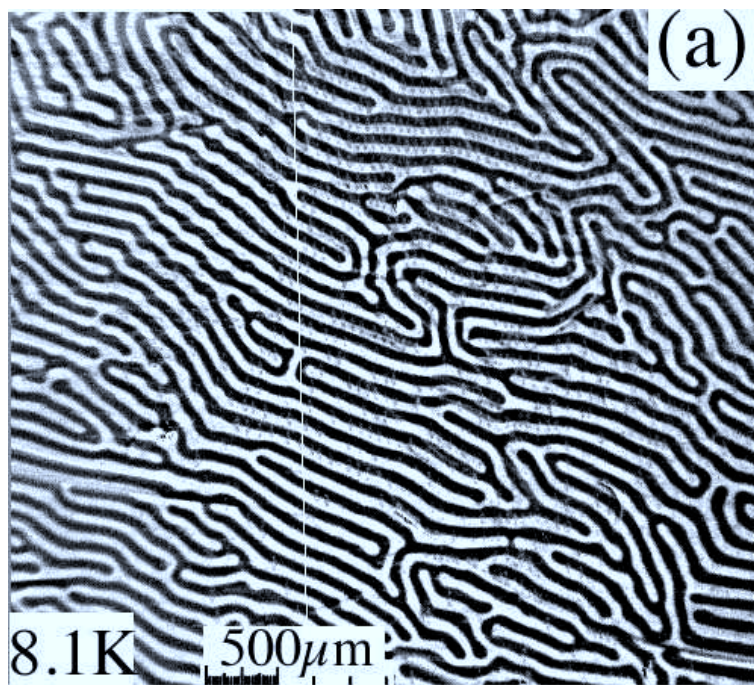


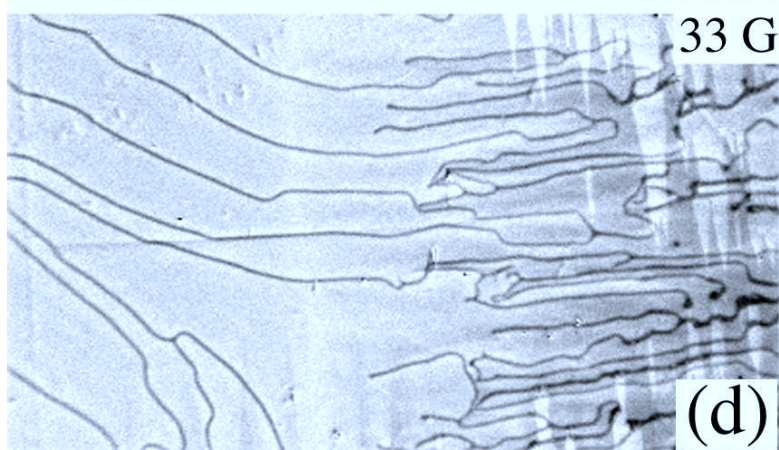
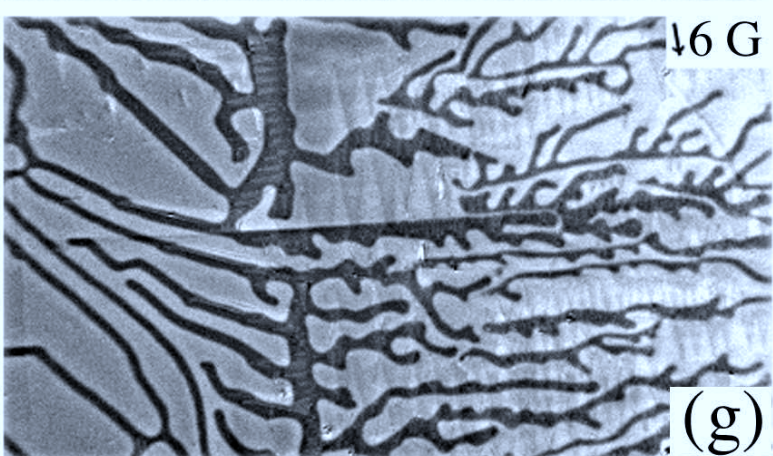
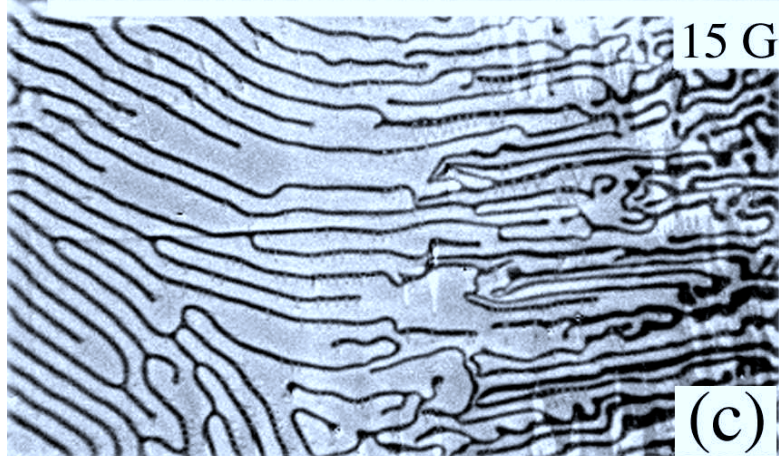
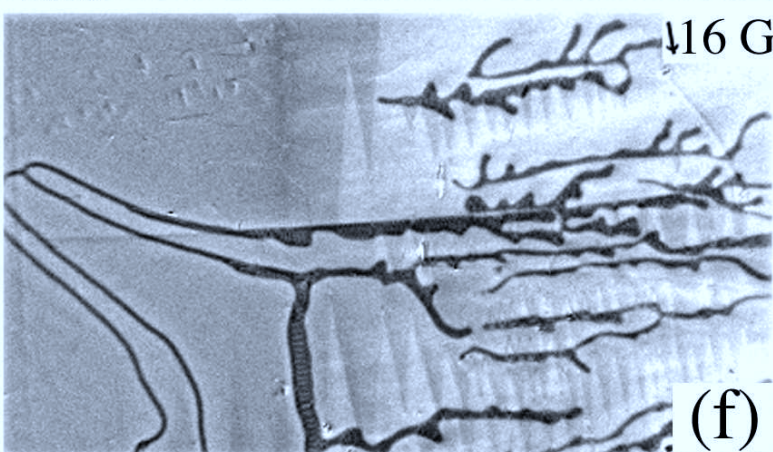
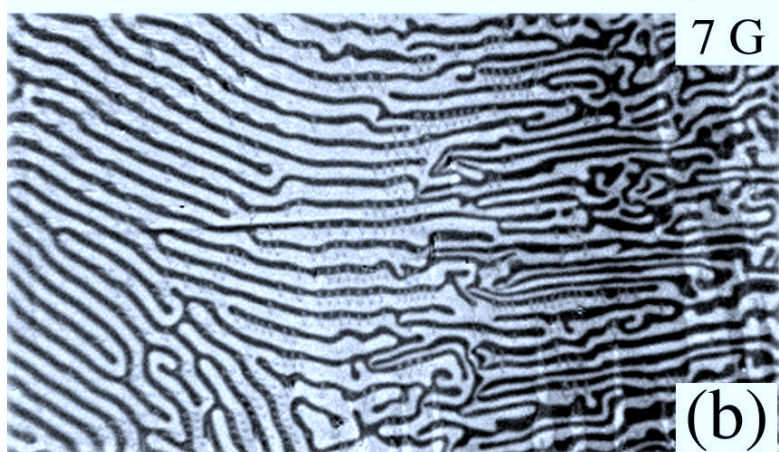
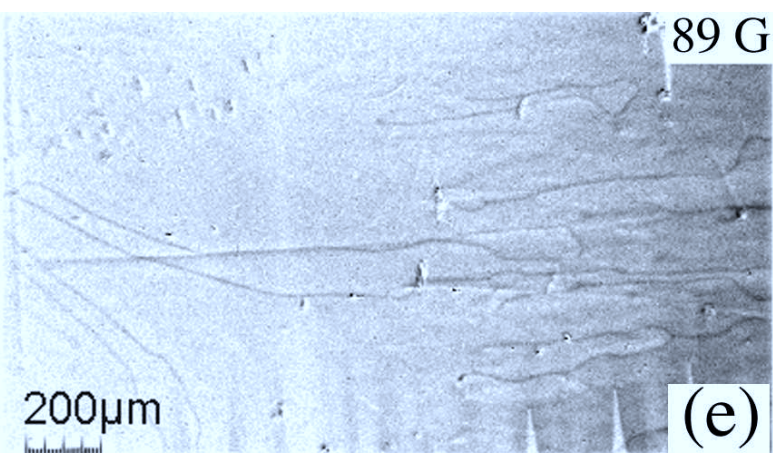
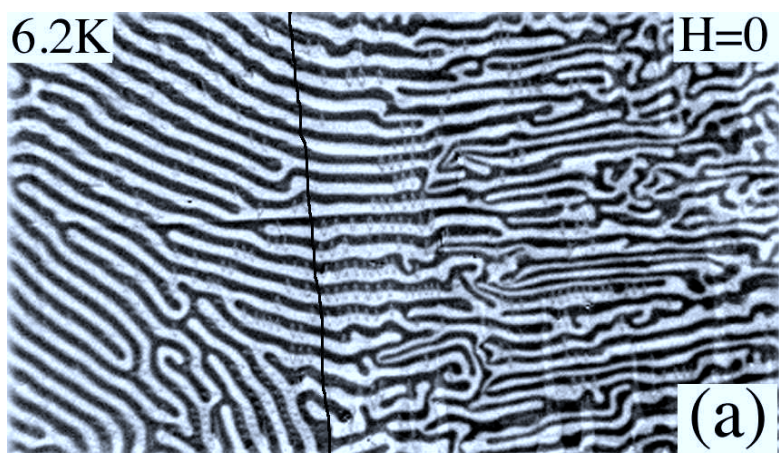


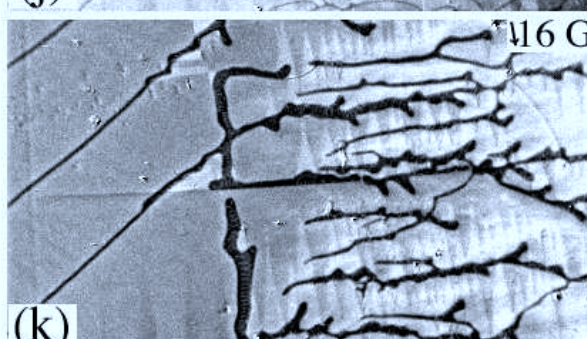
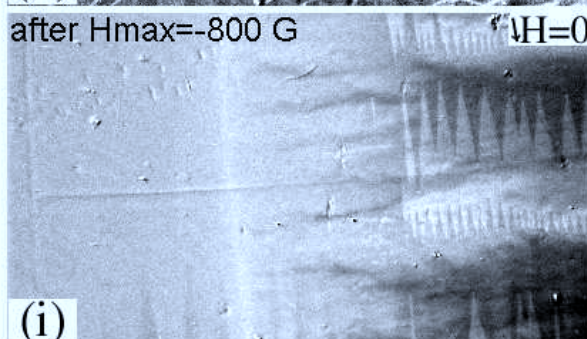
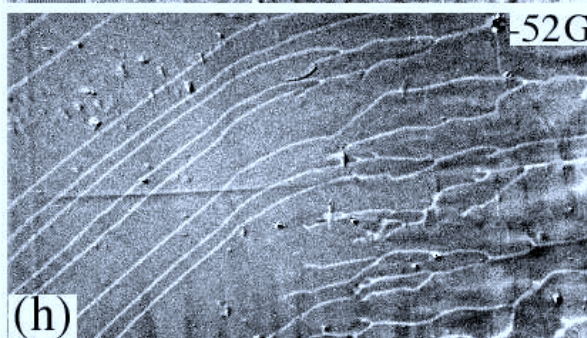
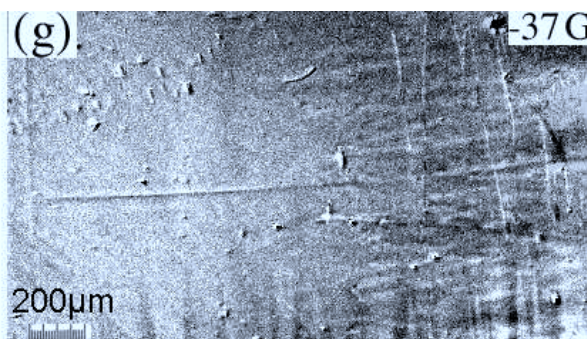
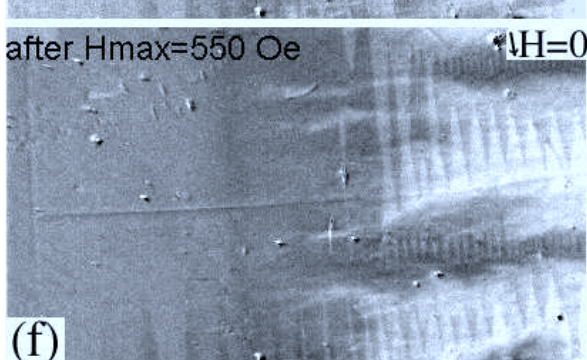
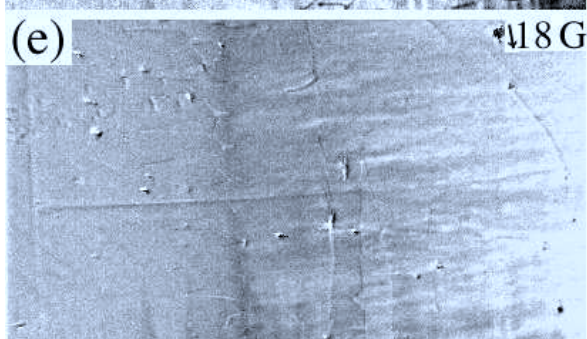
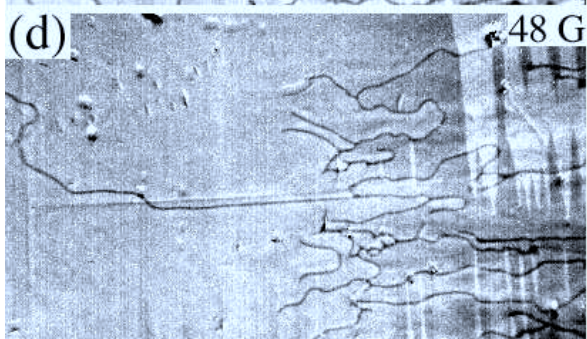
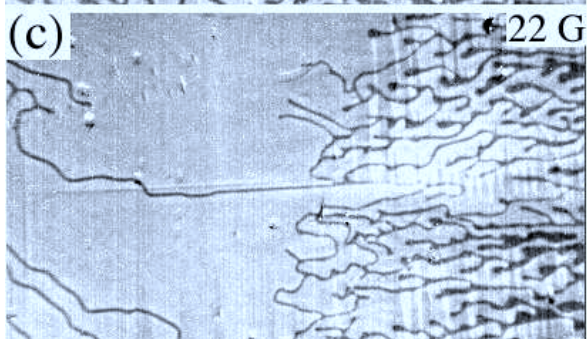
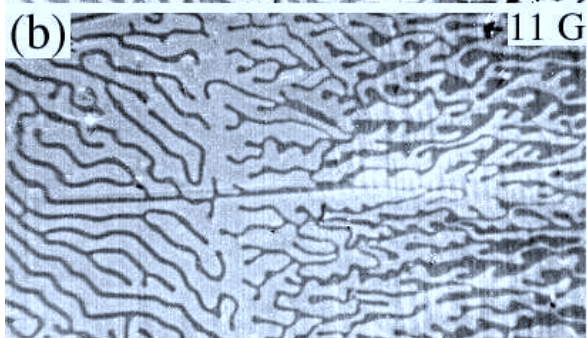
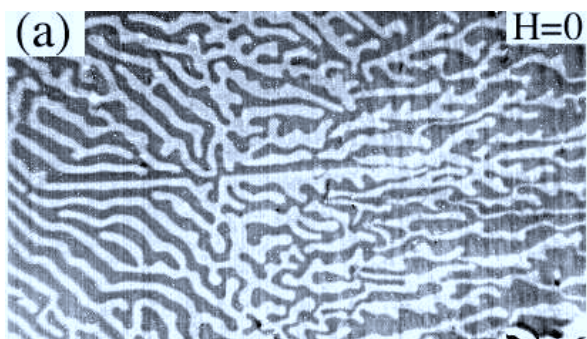


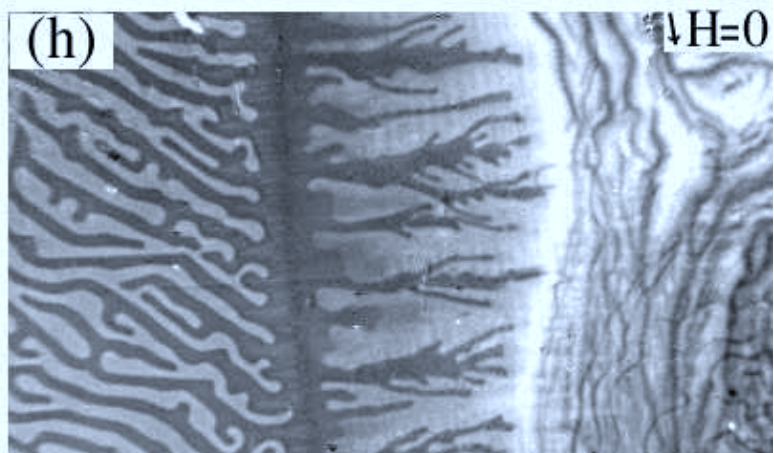
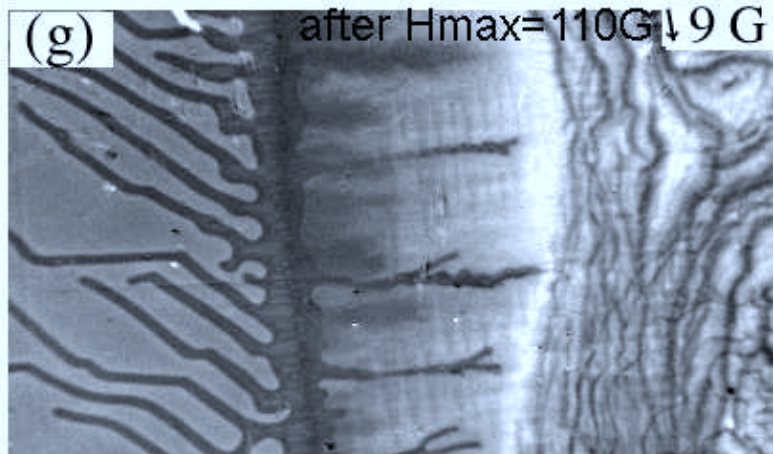
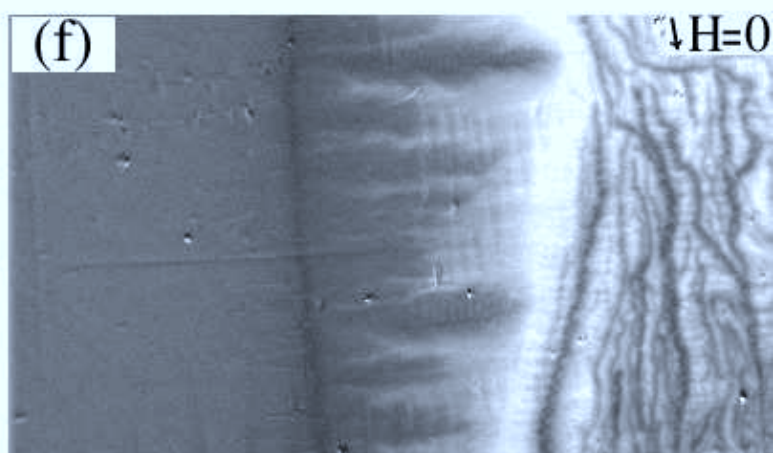
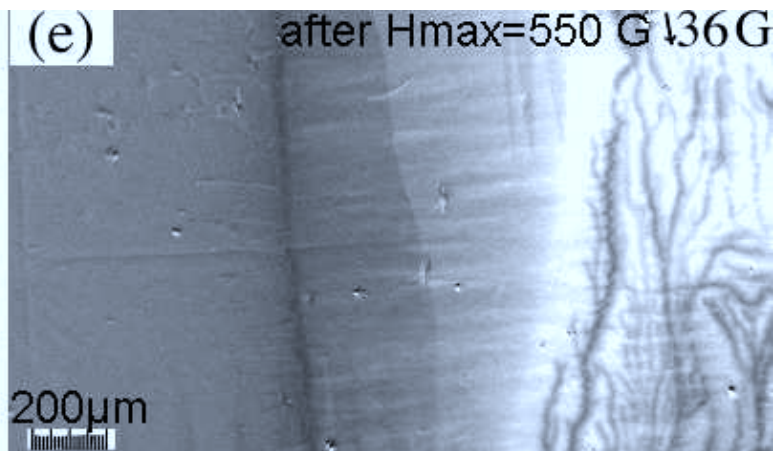
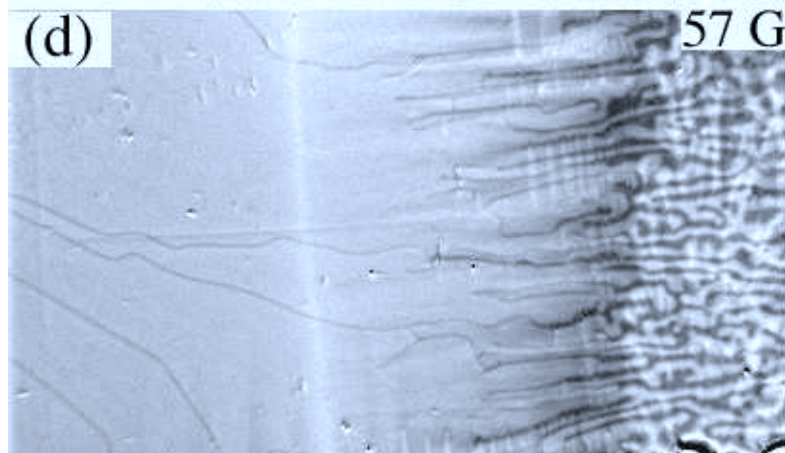
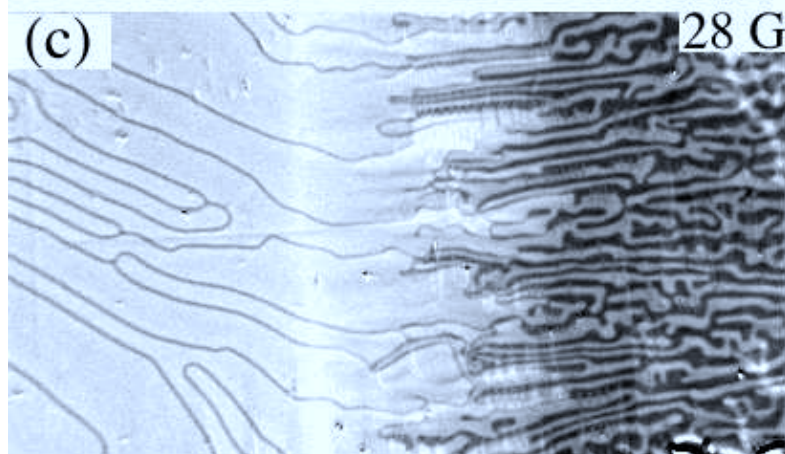
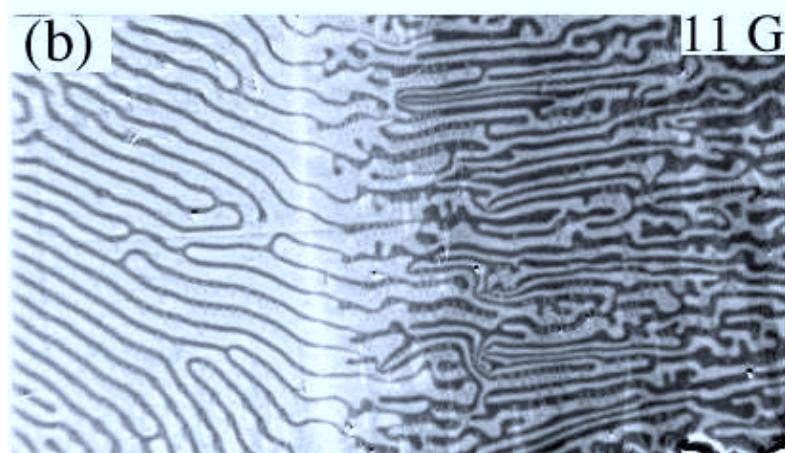


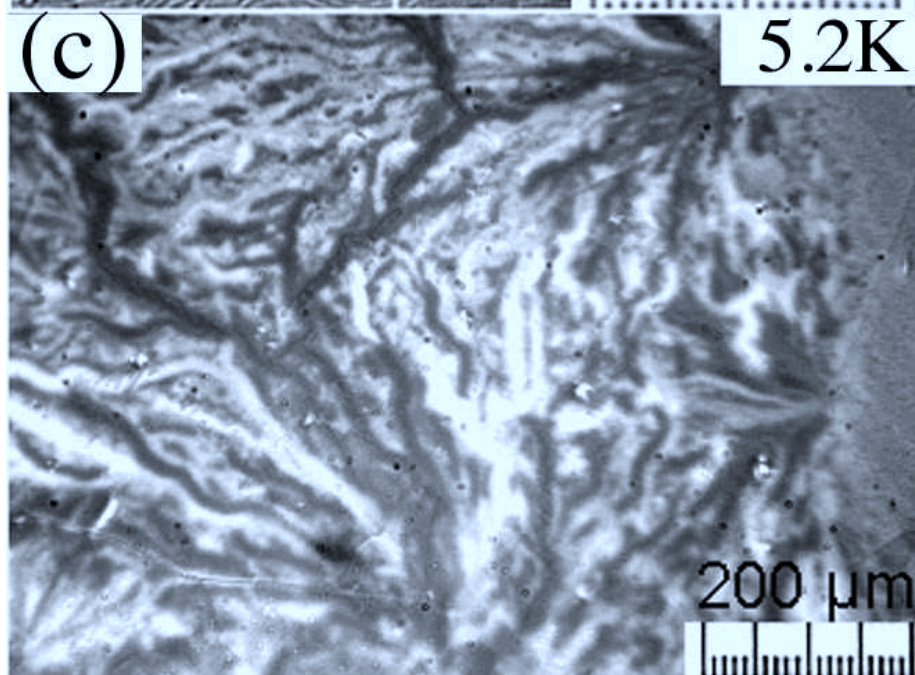
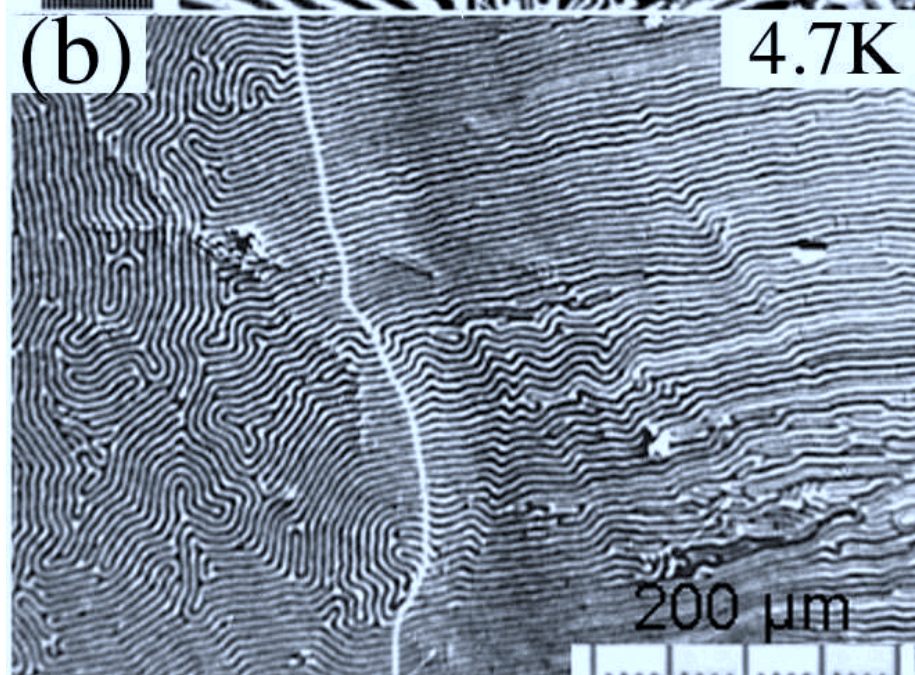
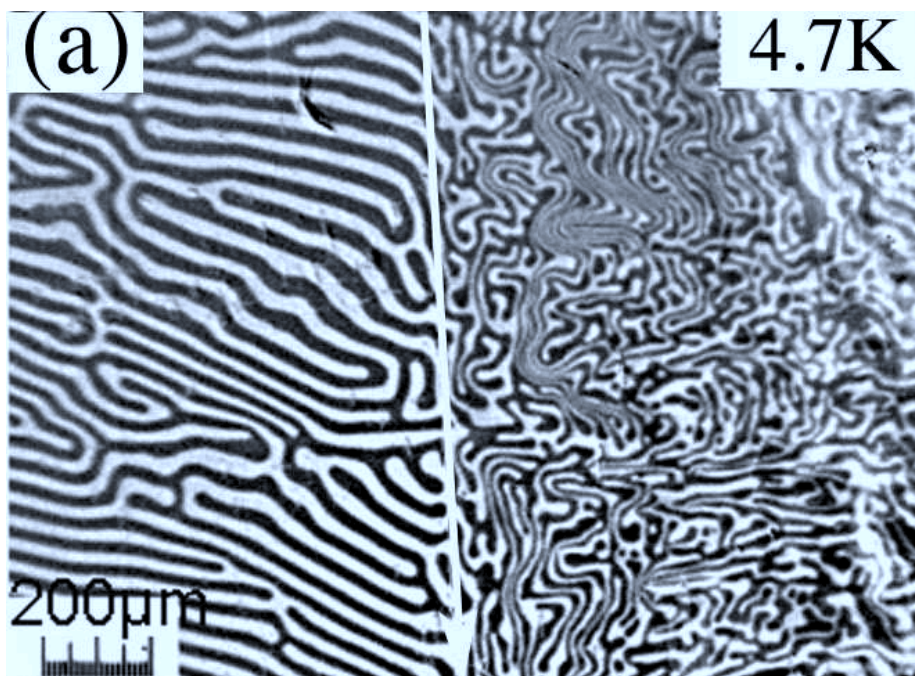


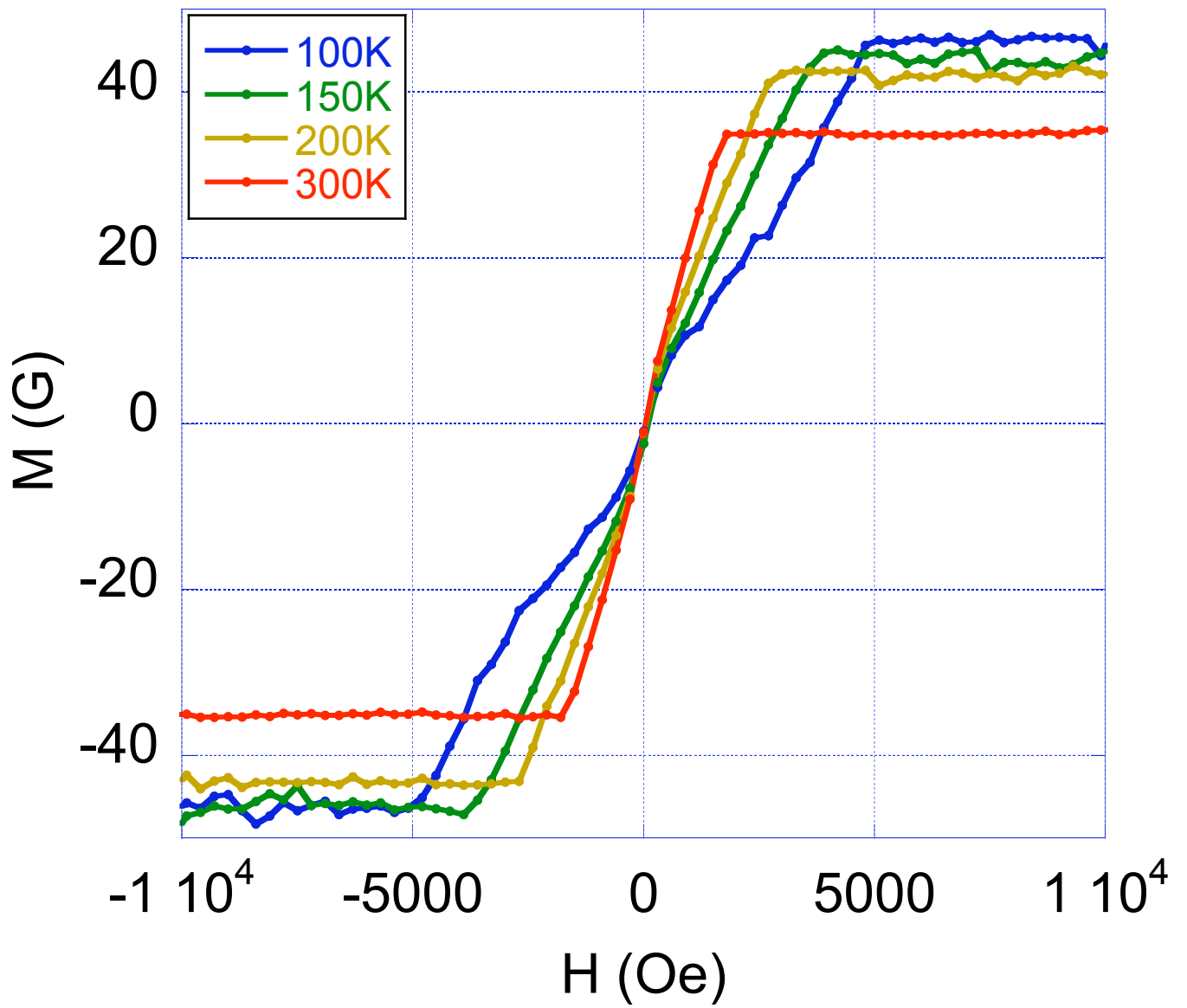


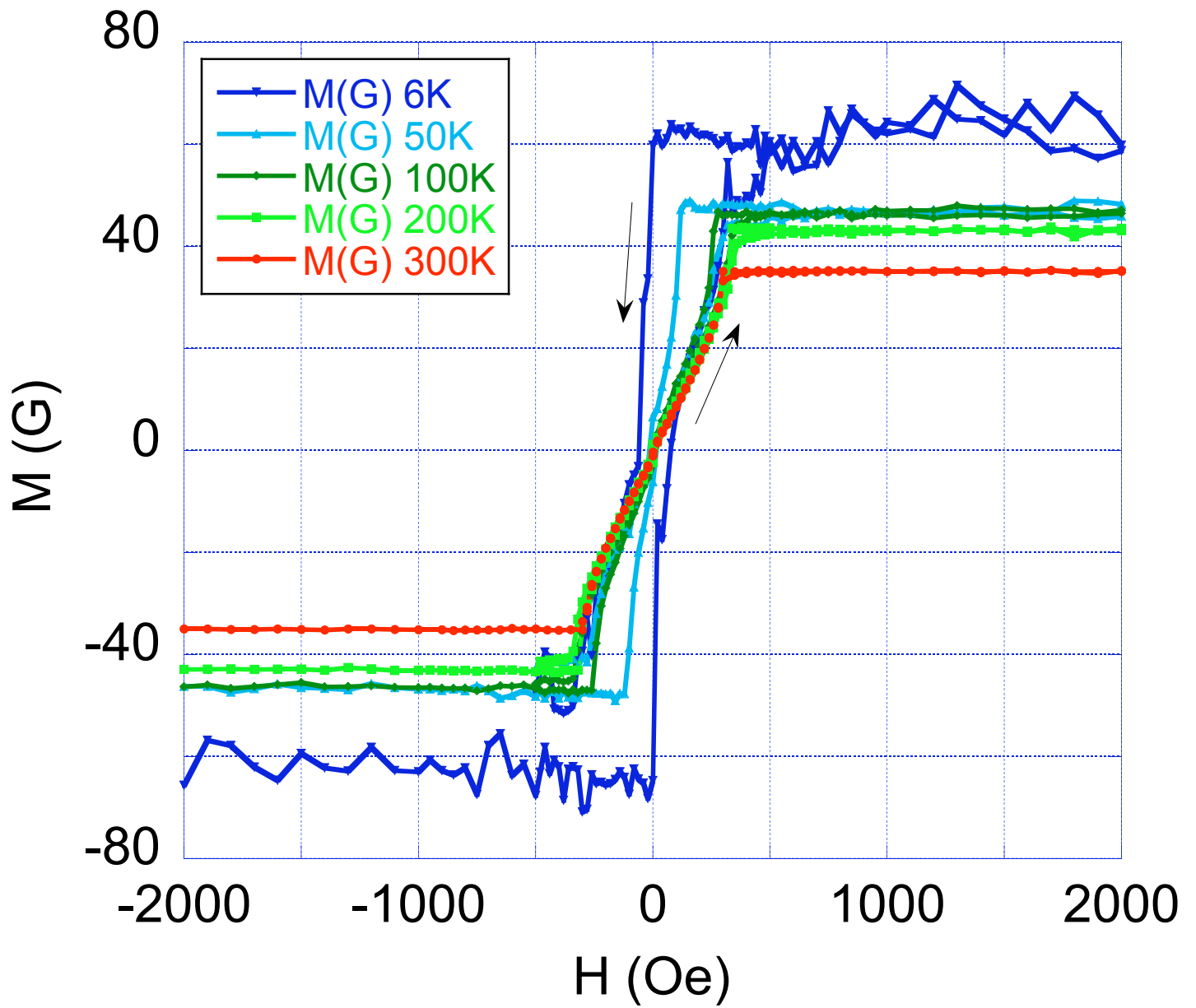


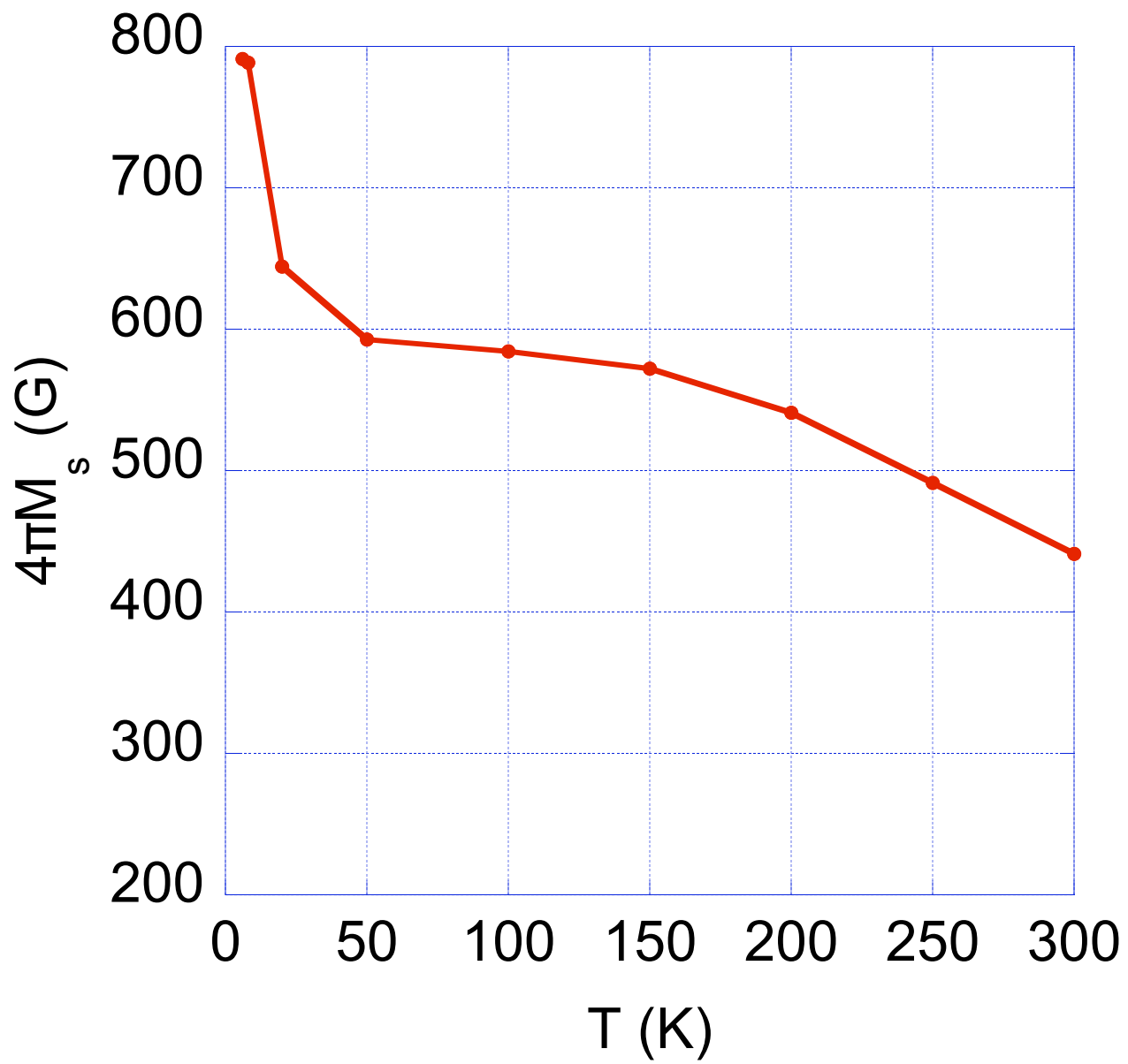


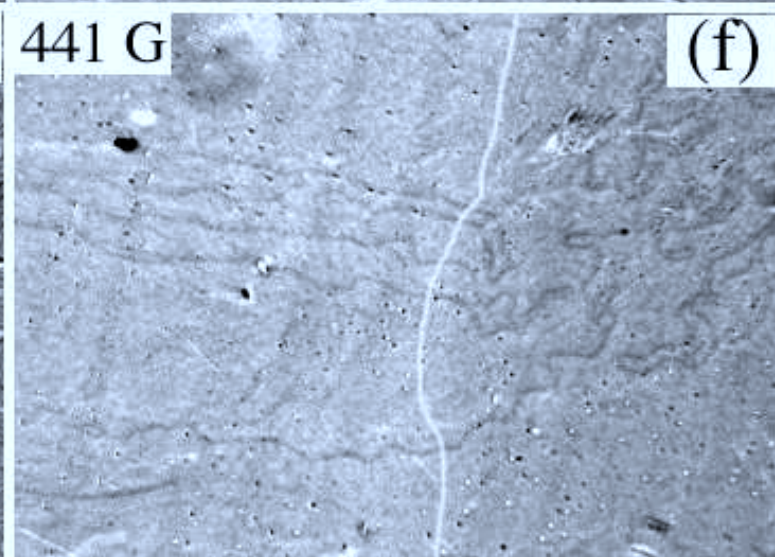
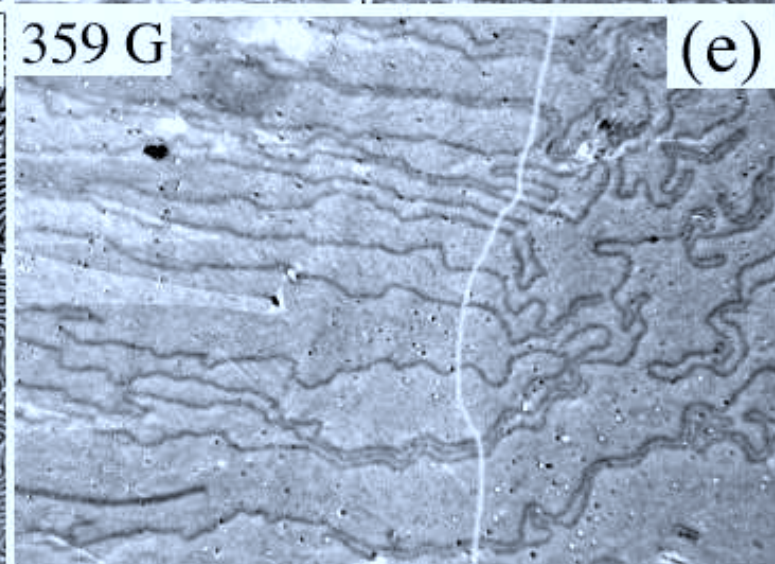
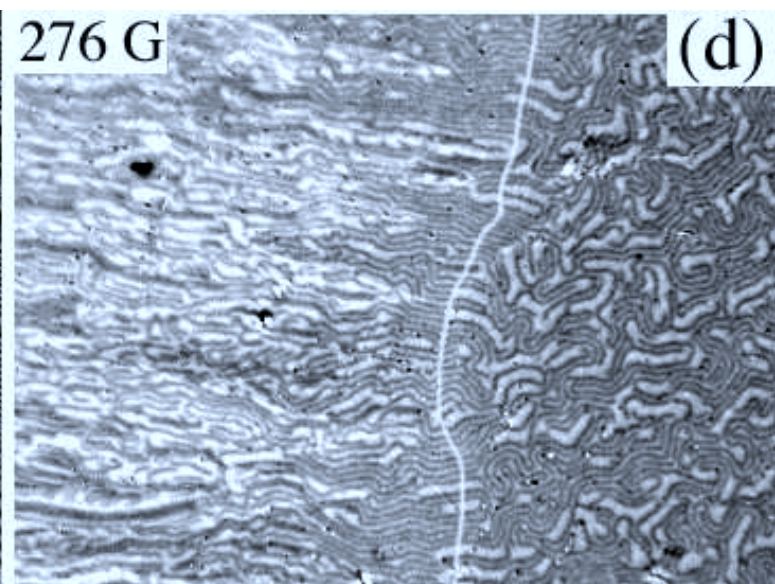
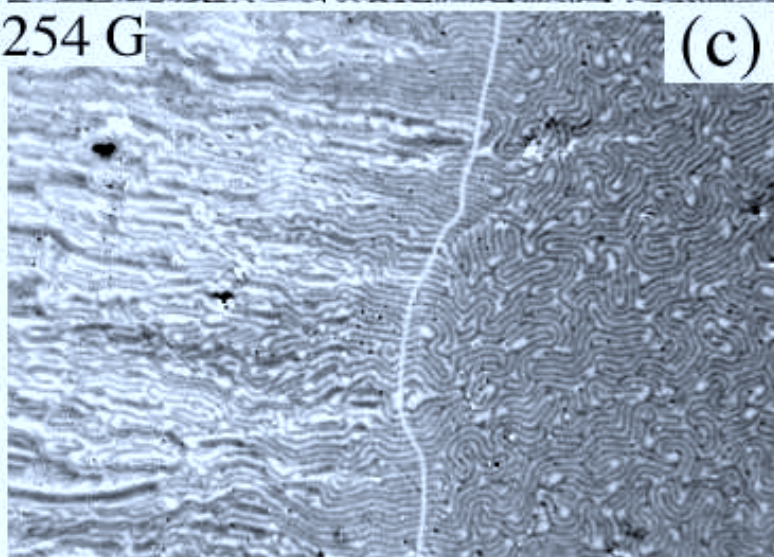
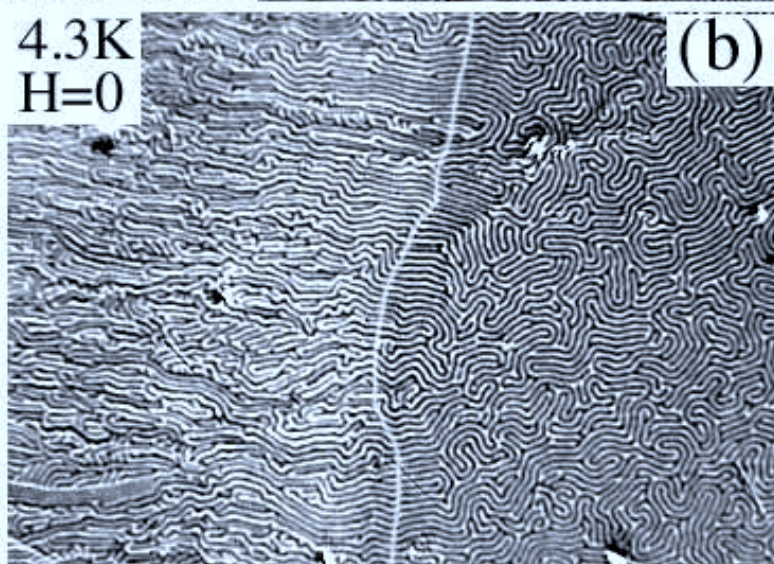
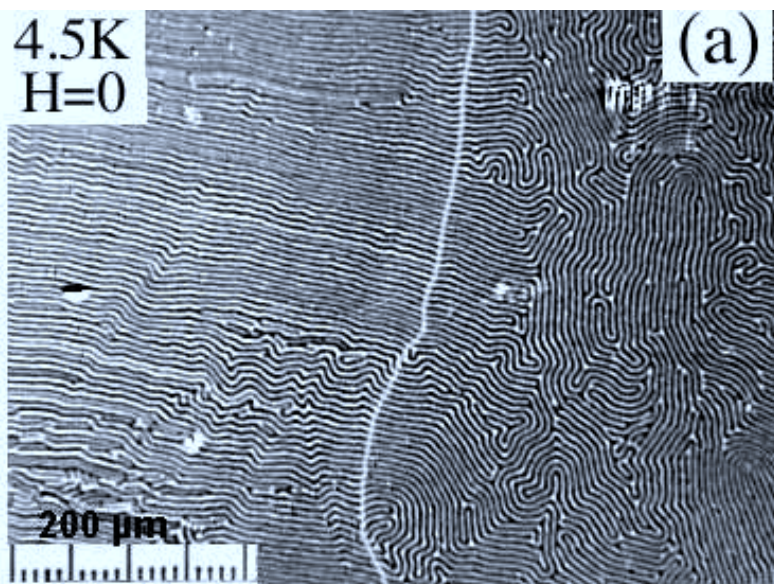


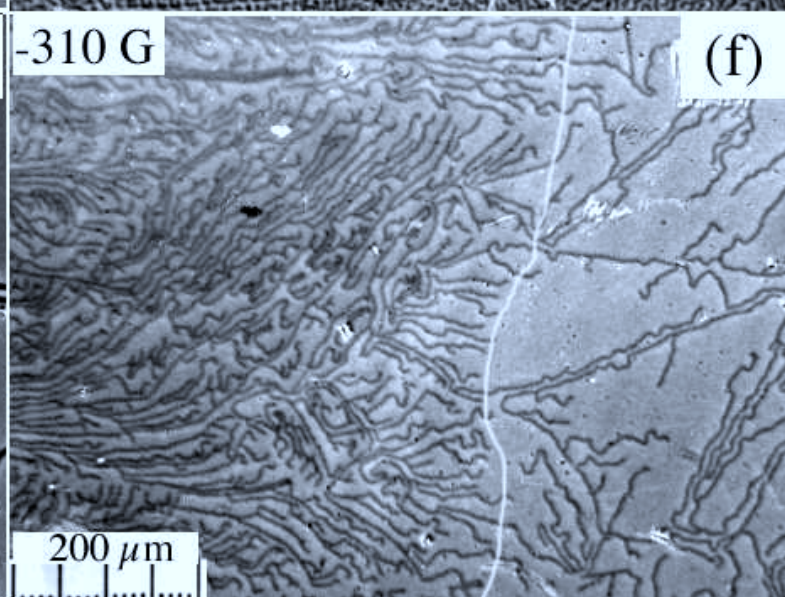
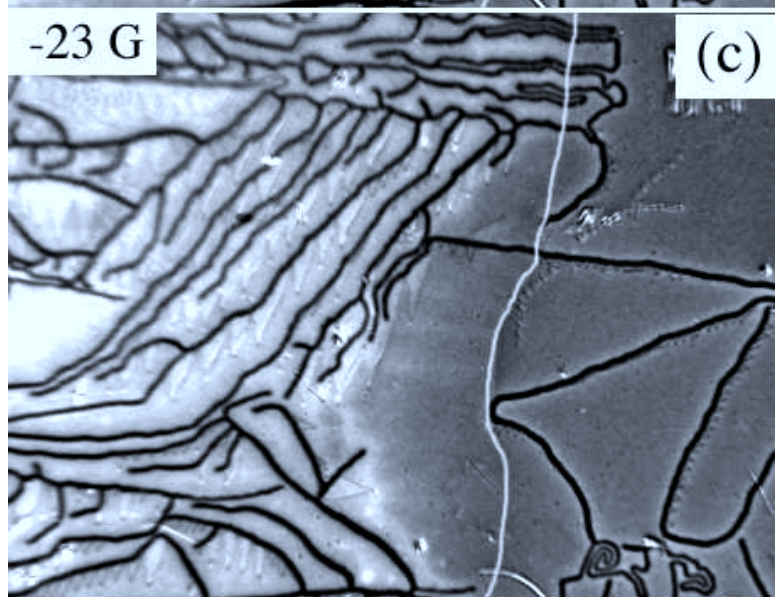
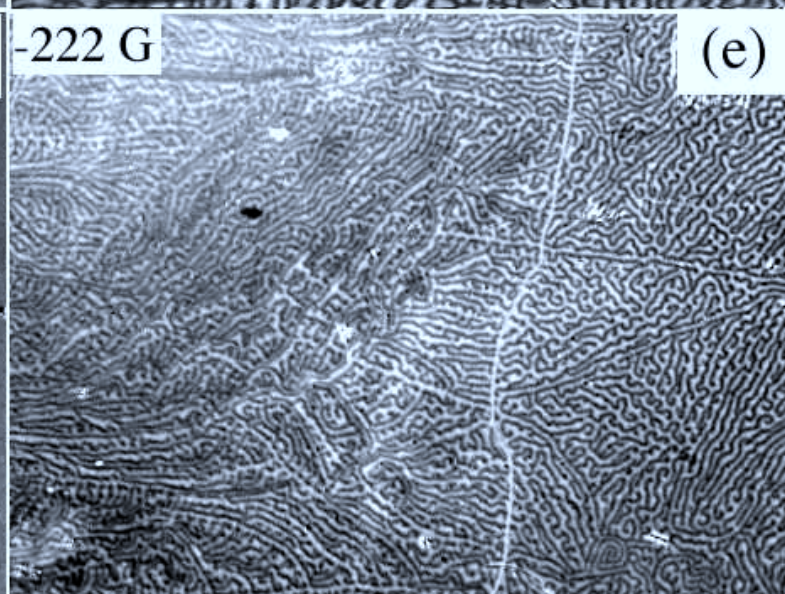
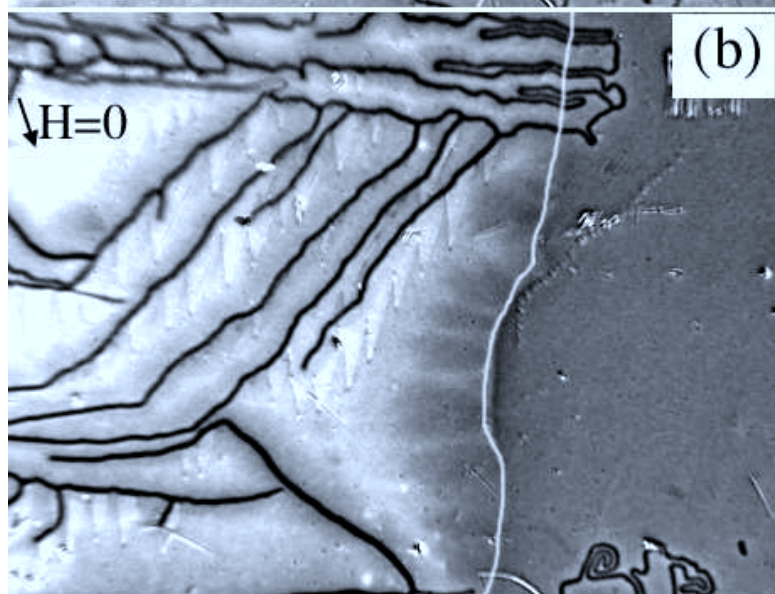
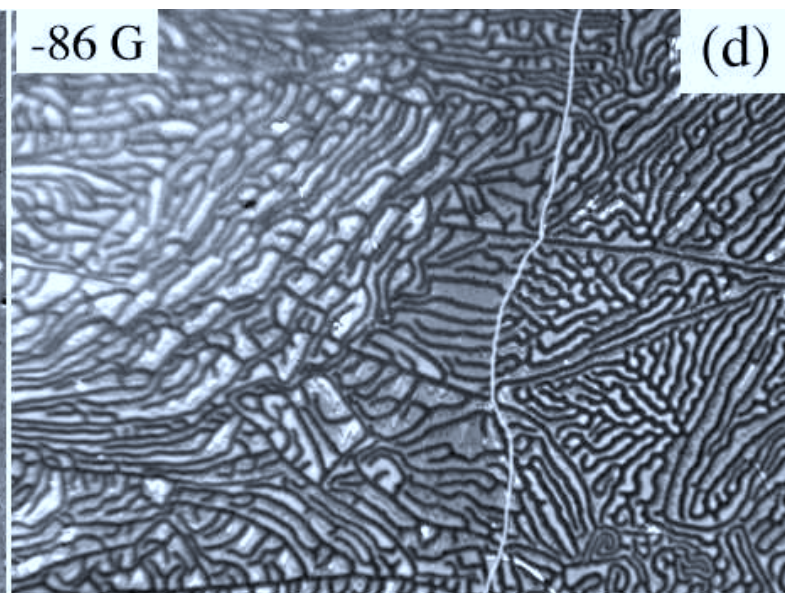
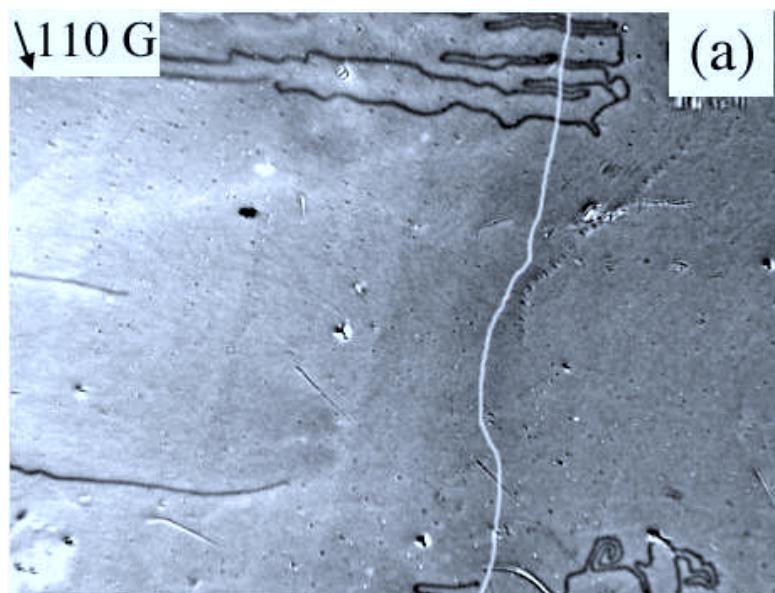


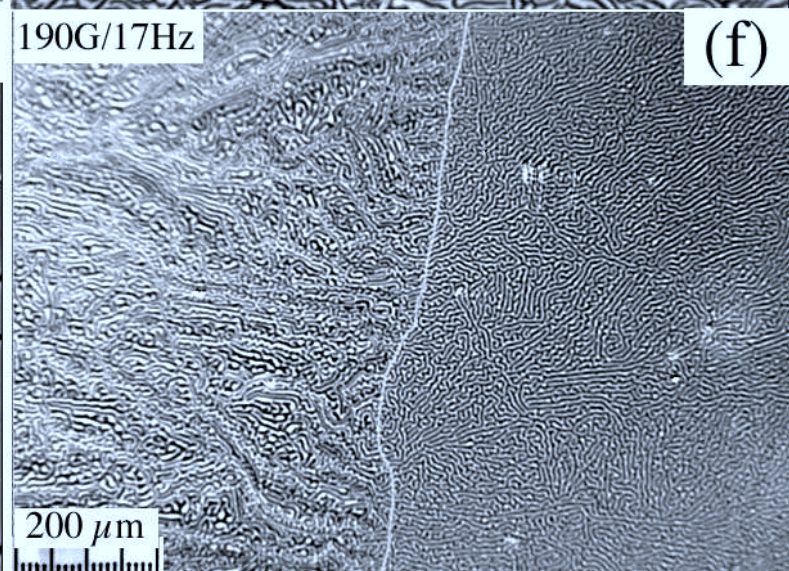
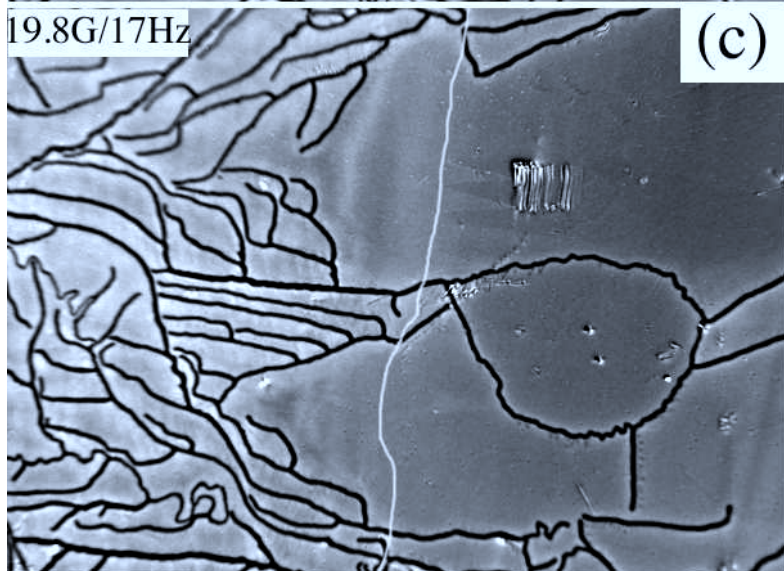
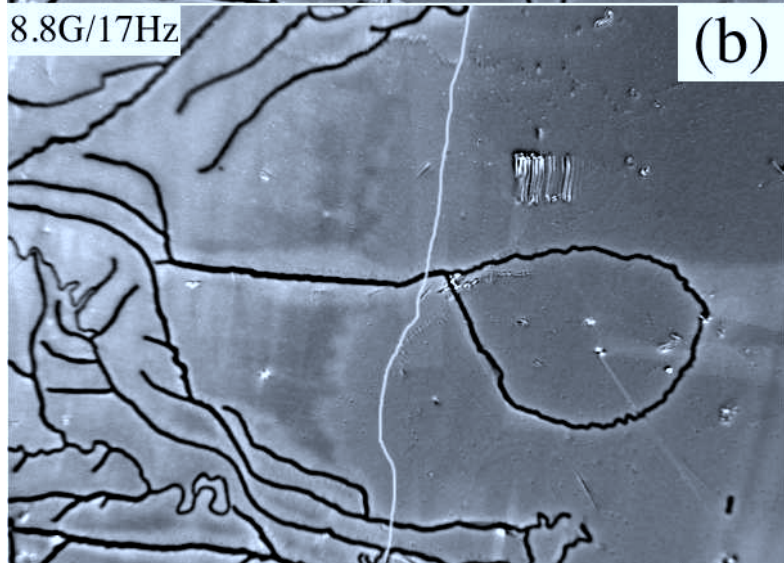
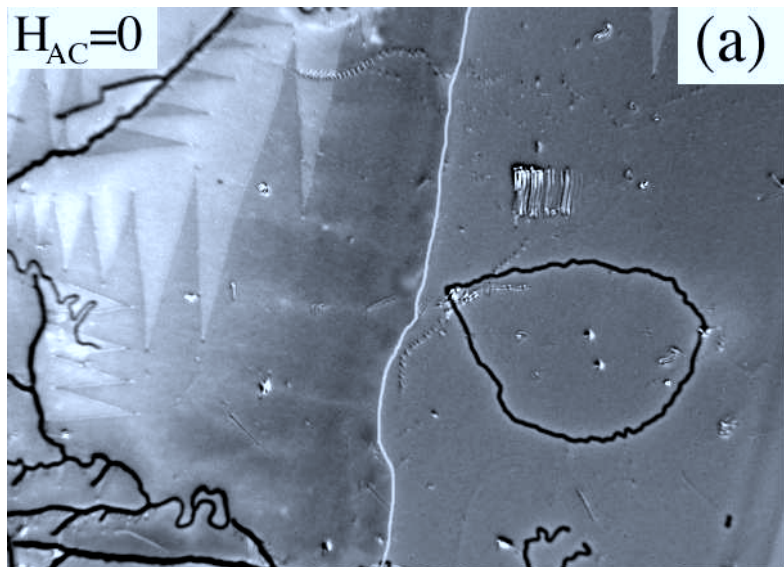


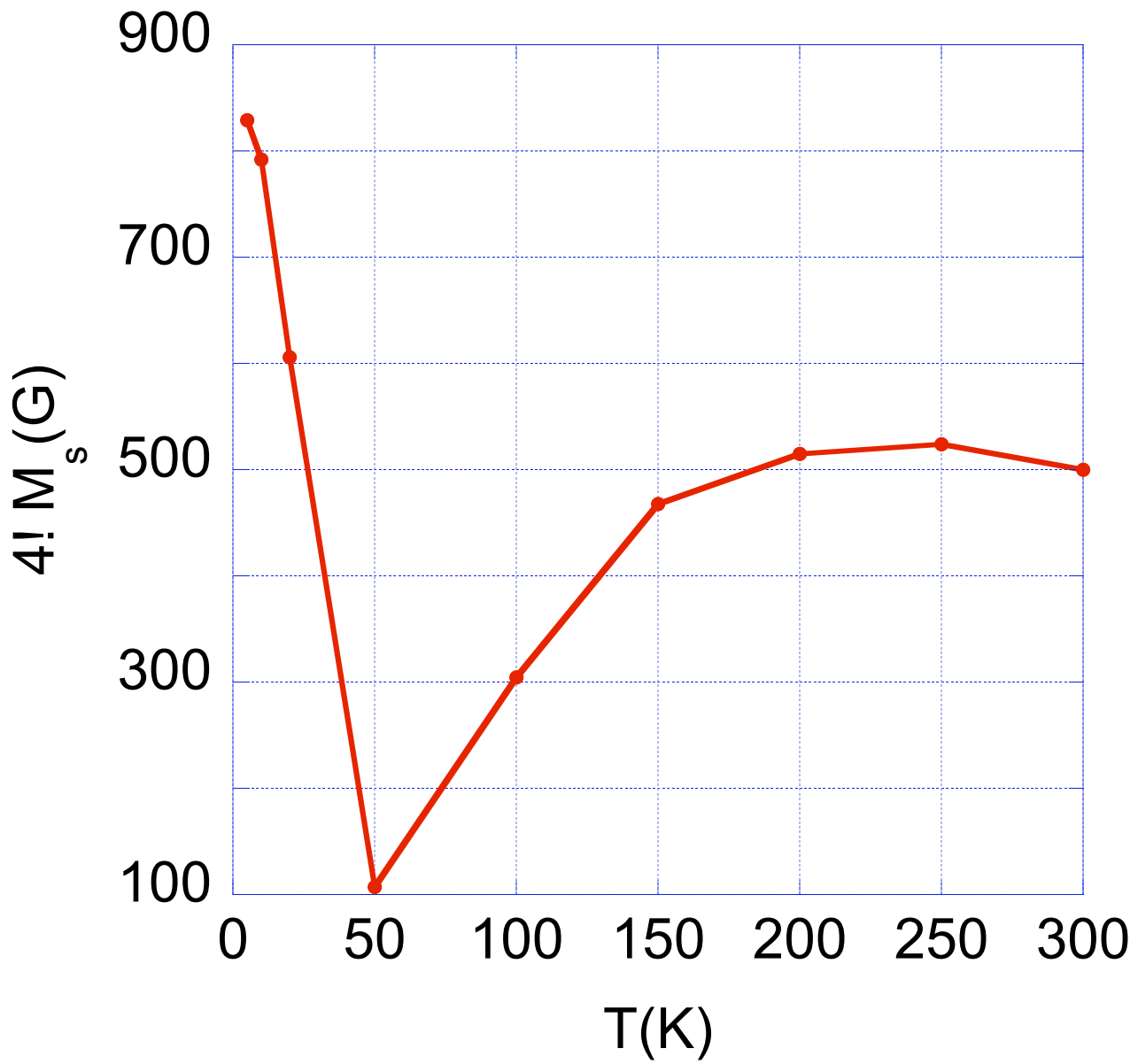


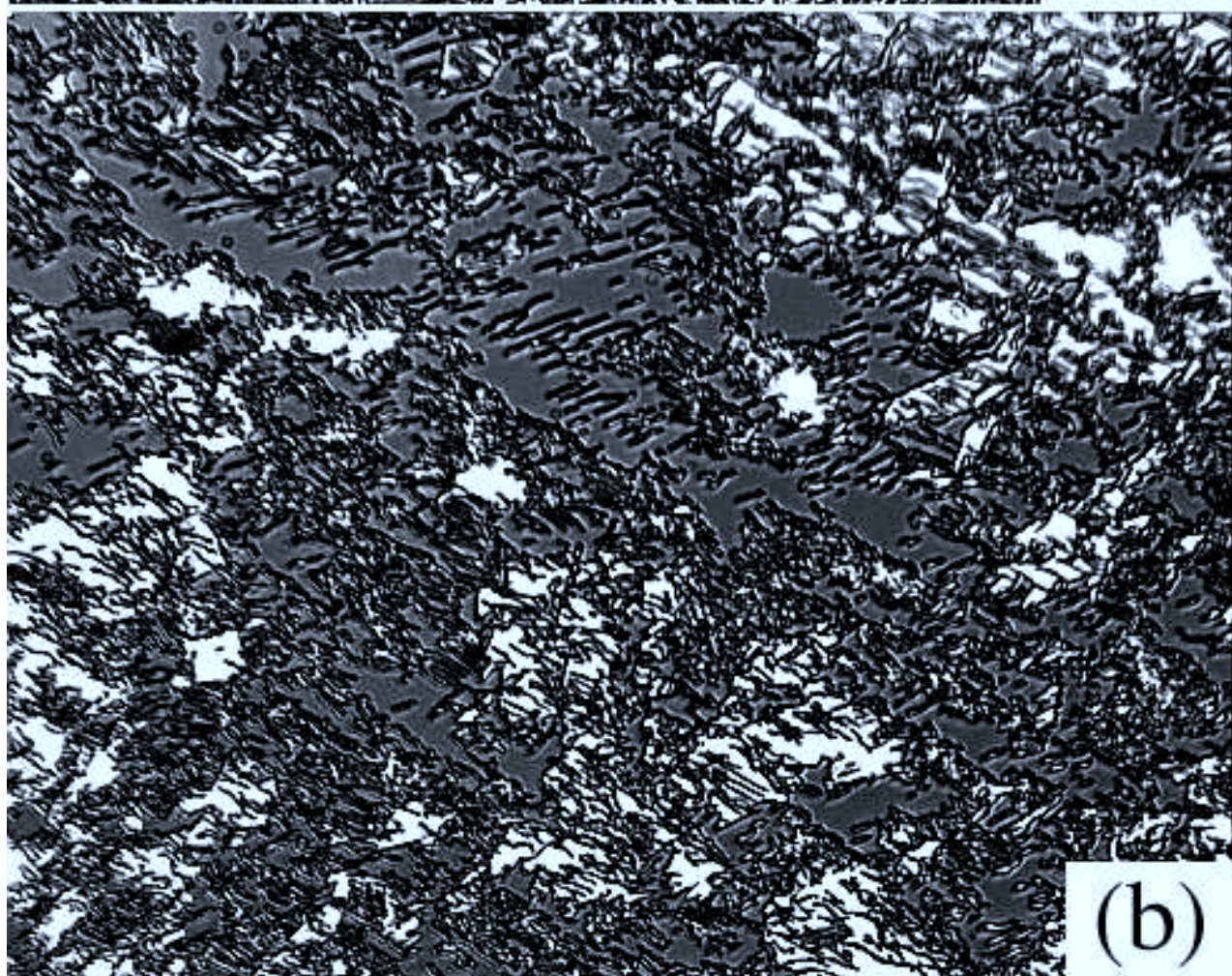
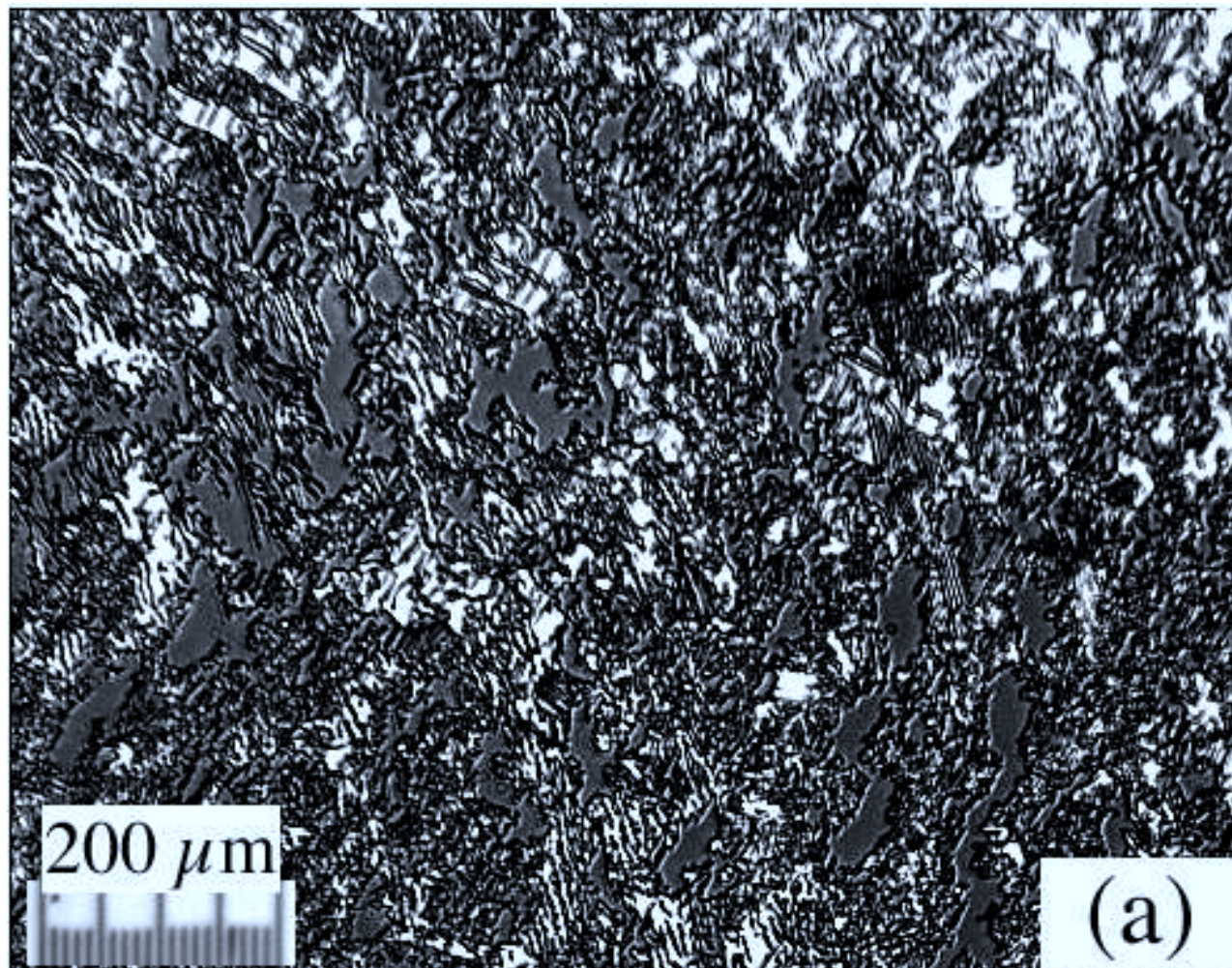


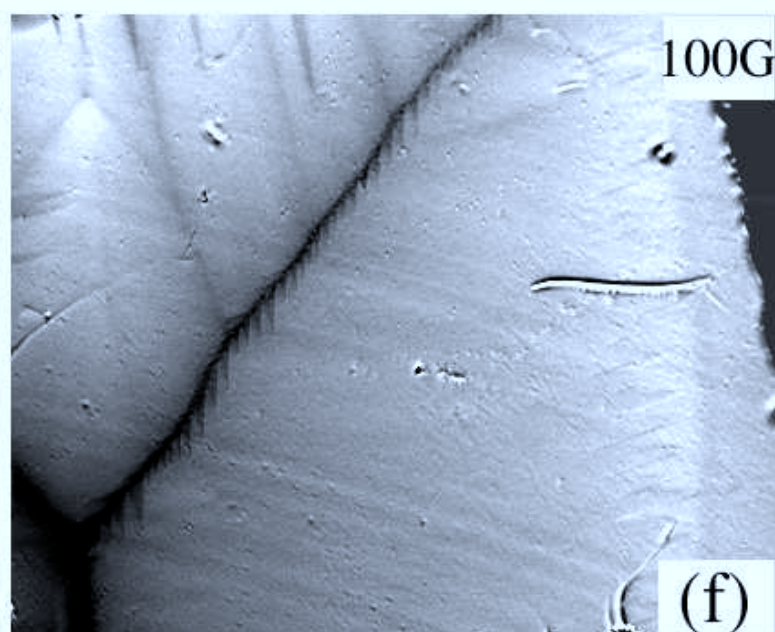
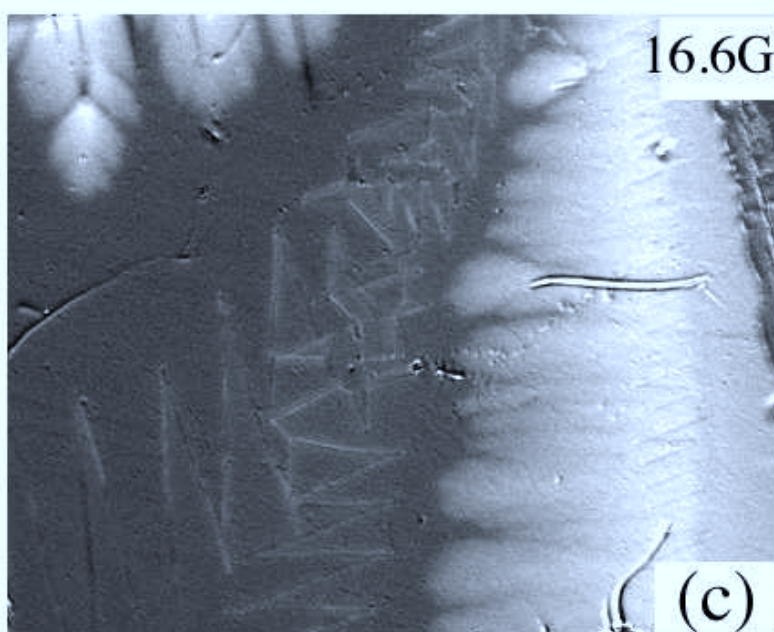
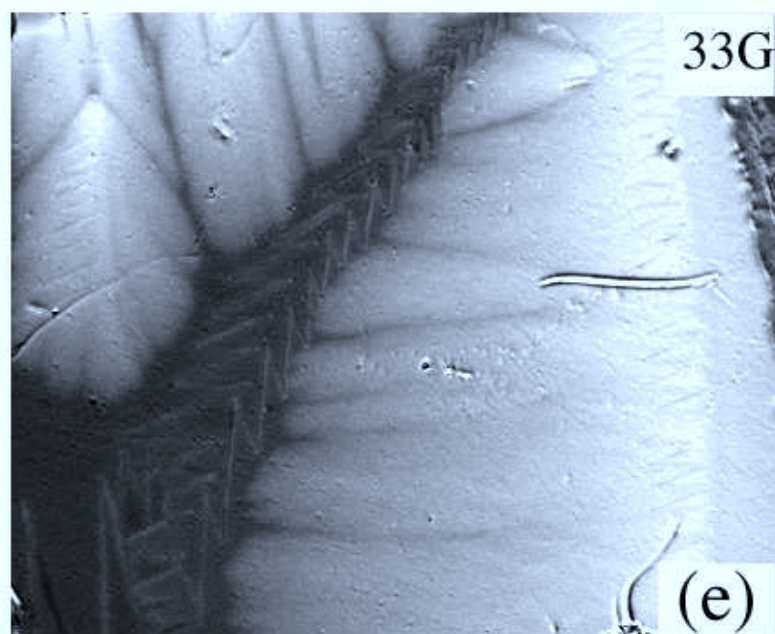
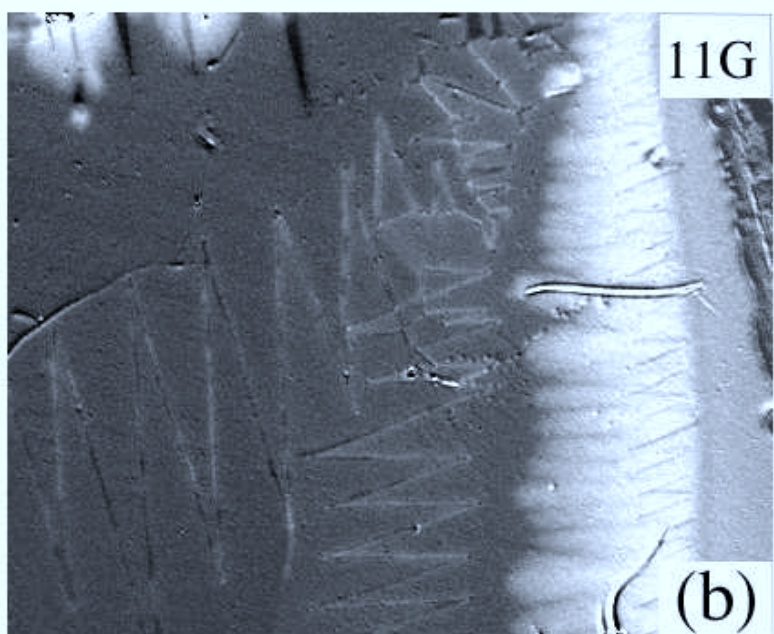
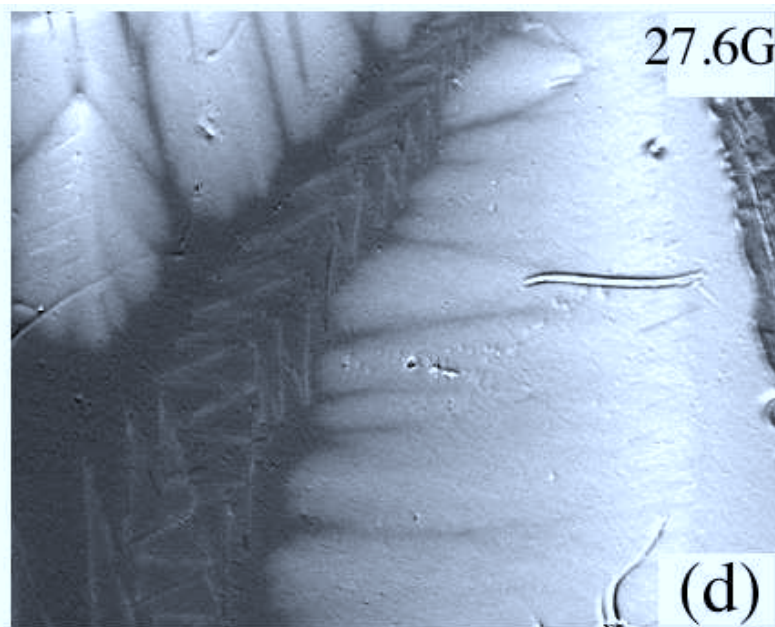
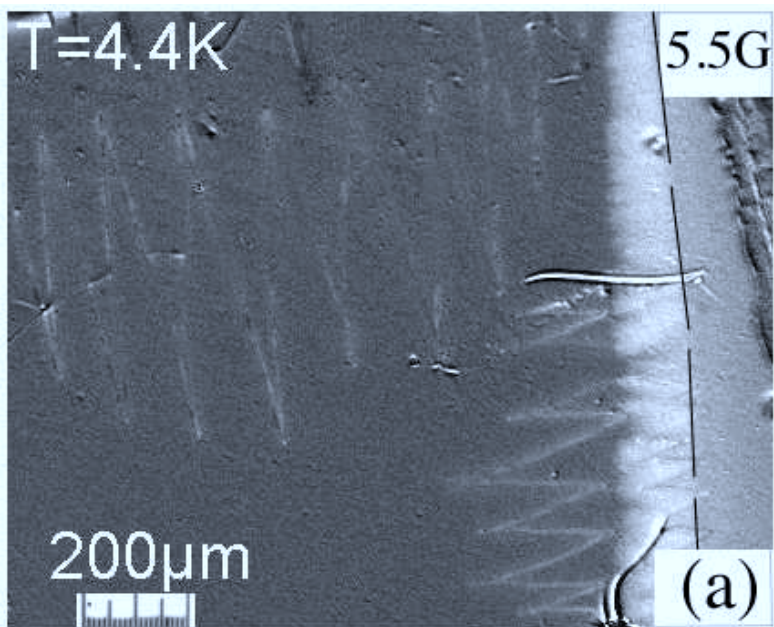




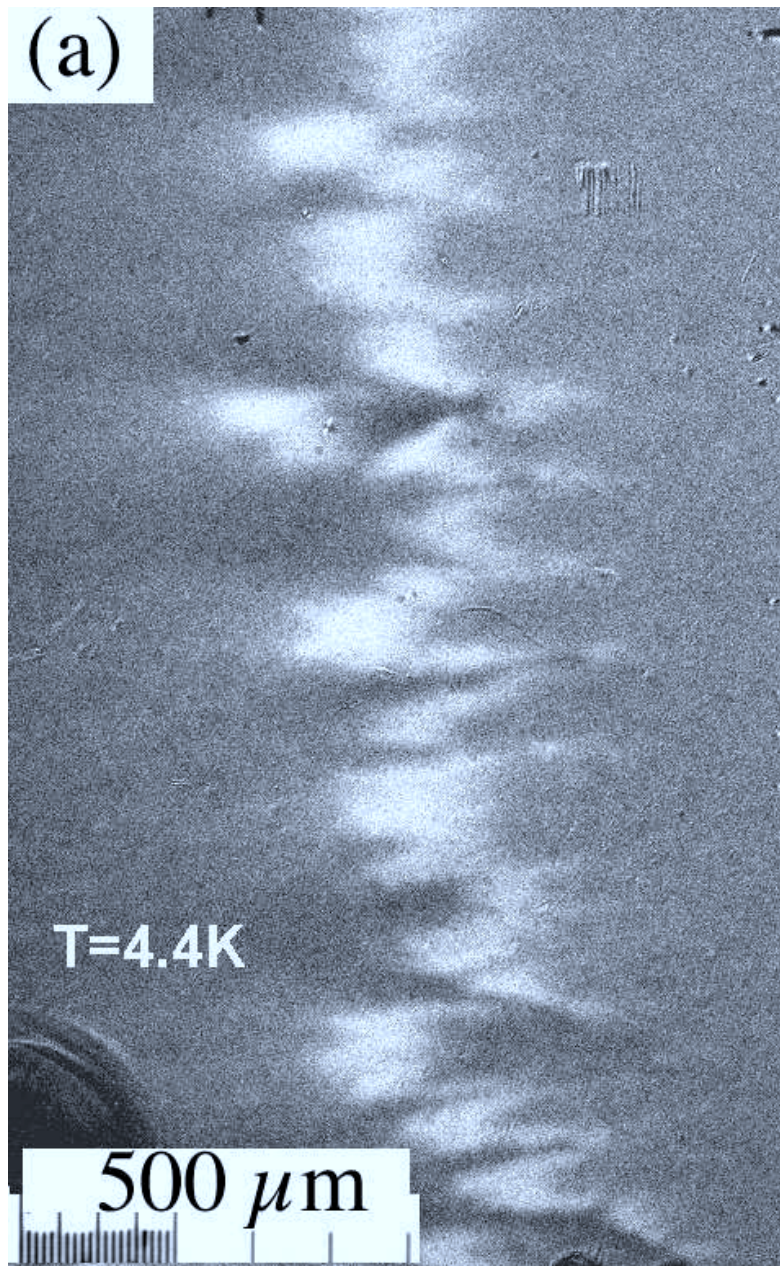




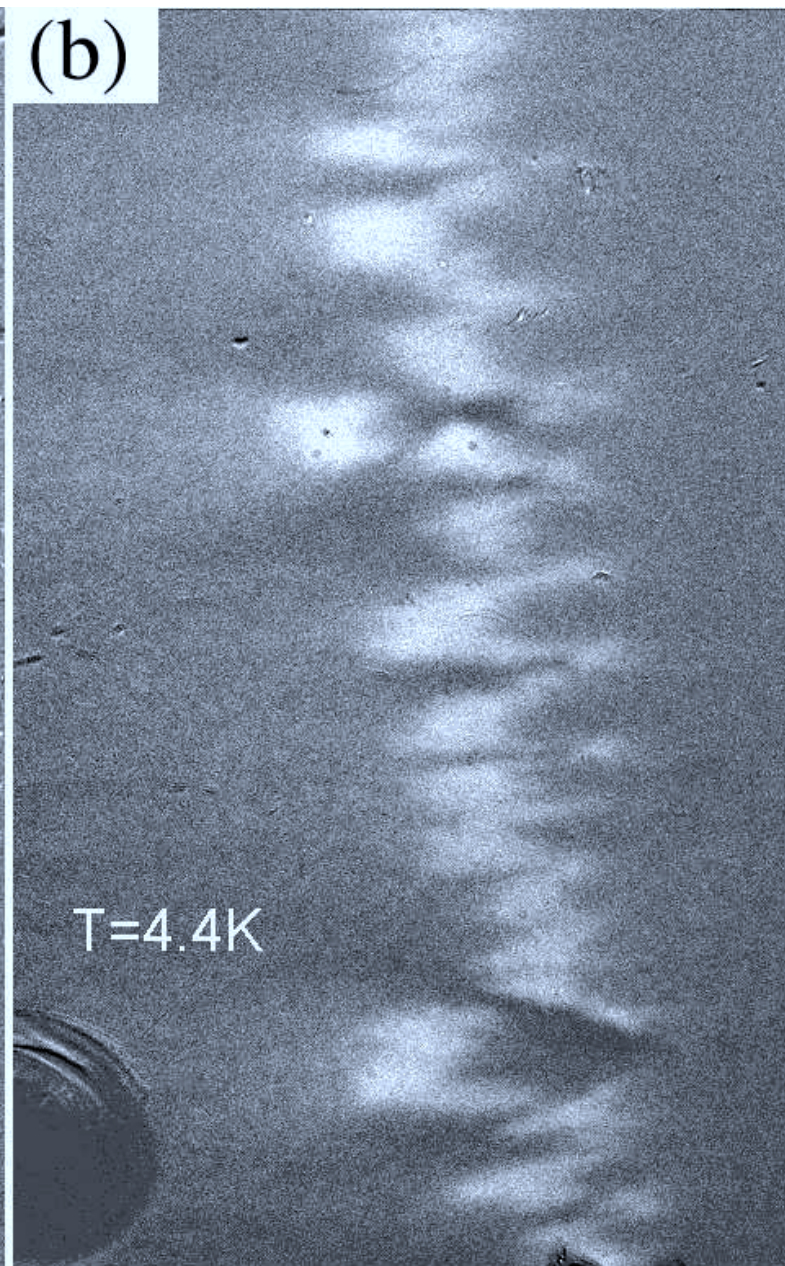


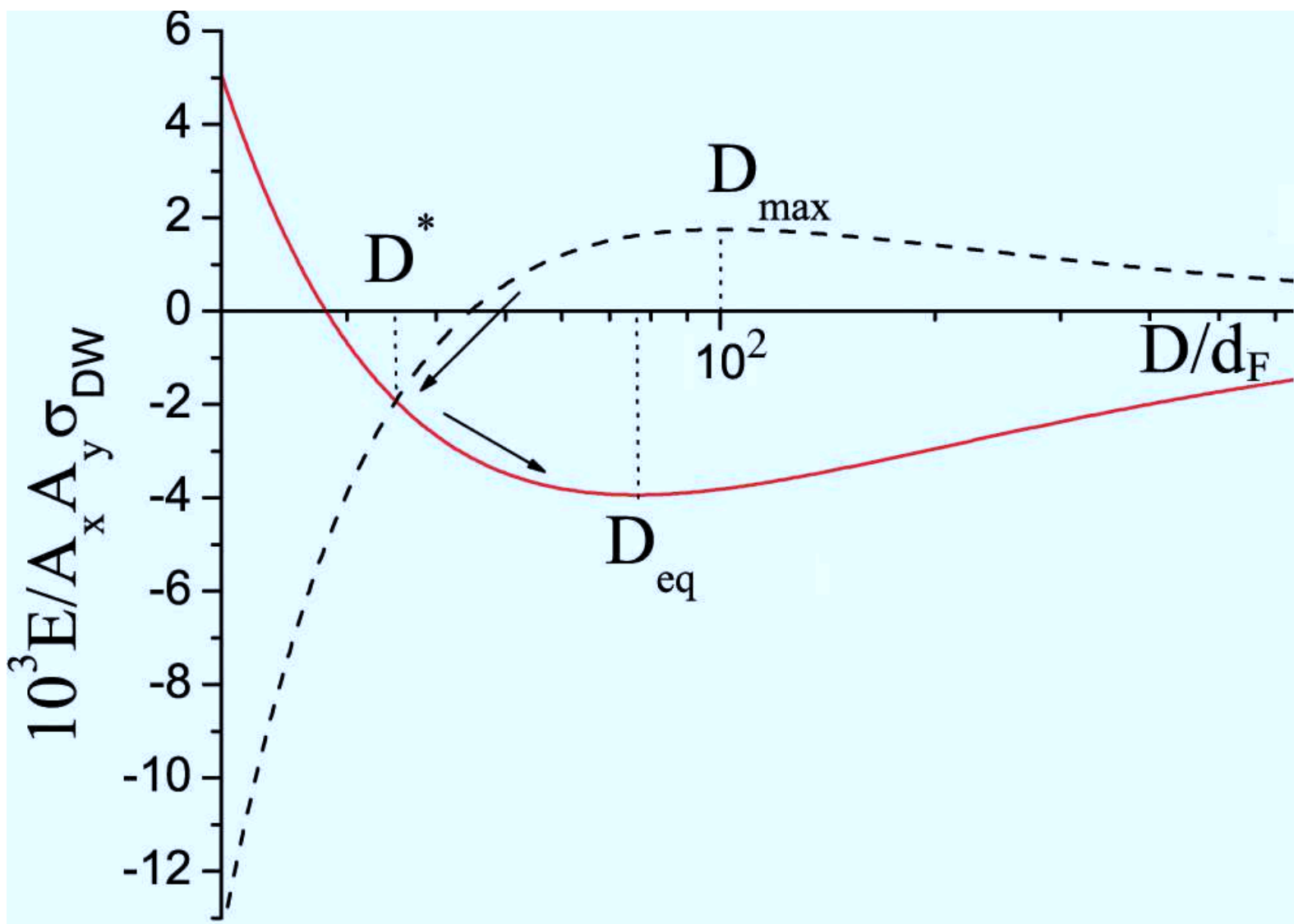


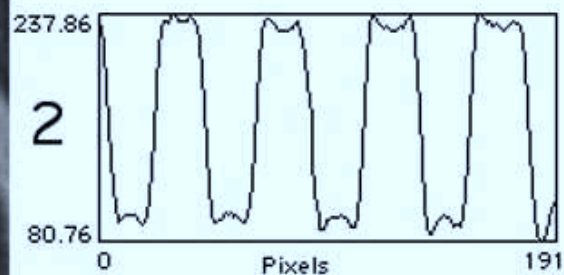
(a)



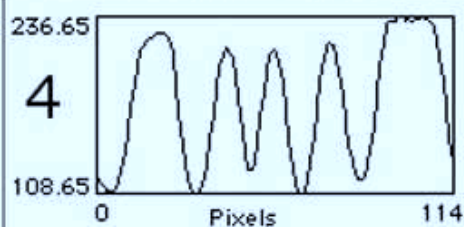
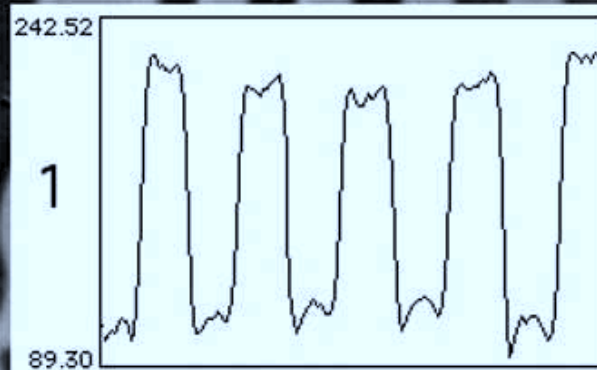
(b)







Nb edge



200  $\mu\text{m}$